



**CHALMERS**  
UNIVERSITY OF TECHNOLOGY

## **GPUMD 4.0: A high-performance molecular dynamics package for versatile materials simulations with machine-learned potentials**

Downloaded from: <https://research.chalmers.se>, 2026-04-15 06:23 UTC

Citation for the original published paper (version of record):

Xu, K., Bu, H., Pan, S. et al (2025). GPUMD 4.0: A high-performance molecular dynamics package for versatile materials simulations with machine-learned potentials. *MATERIALS GENOME ENGINEERING ADVANCES*, 3(3). <http://dx.doi.org/10.1002/mgea.70028>

N.B. When citing this work, cite the original published paper.

## REVIEW

# GPUMD 4.0: A high-performance molecular dynamics package for versatile materials simulations with machine-learned potentials

Ke Xu<sup>1</sup> | Hekai Bu<sup>2</sup> | Shuning Pan<sup>3</sup> | Eric Lindgren<sup>4</sup> | Yongchao Wu<sup>5</sup> |  
 Yong Wang<sup>3,6</sup> | Jiahui Liu<sup>7</sup> | Keke Song<sup>7</sup> | Bin Xu<sup>8</sup> | Yifan Li<sup>6</sup> | Tobias Hainer<sup>4</sup> |  
 Lucas Svensson<sup>4</sup> | Julia Wiktor<sup>4</sup> | Rui Zhao<sup>9</sup> | Hongfu Huang<sup>10</sup>  | Cheng Qian<sup>11</sup> |  
 Shuo Zhang<sup>12</sup> | Zezhu Zeng<sup>13</sup> | Bohan Zhang<sup>1</sup> | Benrui Tang<sup>1</sup> | Yang Xiao<sup>1</sup> |  
 Zihan Yan<sup>14</sup>  | Jiuyang Shi<sup>3</sup> | Zhixin Liang<sup>3</sup> | Junjie Wang<sup>3</sup> | Ting Liang<sup>15</sup> |  
 Shuo Cao<sup>7</sup> | Yanzhou Wang<sup>16</sup> | Penghua Ying<sup>17</sup> | Nan Xu<sup>18</sup> | Chengbing Chen<sup>19</sup> |  
 Yuwen Zhang<sup>20</sup> | Zherui Chen<sup>21,22</sup> | Xin Wu<sup>23</sup> | Wenwu Jiang<sup>2</sup> | Esme Berger<sup>4</sup> |  
 Yanlong Li<sup>24</sup> | Shunda Chen<sup>25</sup> | Alexander J. Gabourie<sup>26</sup> | Haikuan Dong<sup>1</sup> |  
 Shiyun Xiong<sup>27</sup> | Ning Wei<sup>12</sup> | Yue Chen<sup>13</sup> | Jianbin Xu<sup>15</sup> | Feng Ding<sup>11</sup> |  
 Zhimei Sun<sup>10</sup>  | Tapio Ala-Nissila<sup>16,28</sup> | Ari Harju<sup>29</sup> | Jincheng Zheng<sup>30,31,32</sup> |  
 Pengfei Guan<sup>8</sup> | Paul Erhart<sup>4,33</sup> | Jian Sun<sup>3</sup> | Wengen Ouyang<sup>2,34</sup> | Yanjing Su<sup>7</sup> |  
 Zheyong Fan<sup>1</sup> 

## Correspondence

Zheyong Fan, Pengfei Guan, Paul Erhart, Jian Sun, Wengen Ouyang, and Yanjing Su.

Email: [brucenju@gmail.com](mailto:brucenju@gmail.com), [pguan@nimte.ac.cn](mailto:pguan@nimte.ac.cn), [erhart@chalmers.se](mailto:erhart@chalmers.se), [jiansun@nju.edu.cn](mailto:jiansun@nju.edu.cn), [w.g.ouyang@whu.edu.cn](mailto:w.g.ouyang@whu.edu.cn), and [yjsu@ustb.edu.cn](mailto:yjsu@ustb.edu.cn)

## Abstract

This paper provides a comprehensive overview of the latest stable release of the graphics processing units molecular dynamics (GPUMD) package, GPUMD 4.0. We begin with a brief review of its development history, starting from the initial version. We then discuss the theoretical foundations for the development of the GPUMD package, including the formulations of the interatomic force, virial and heat current for many-body potentials, the development of the highly efficient and flexible neuroevolution potential (NEP) method, the supported integrators and related operations, the various physical properties that can be calculated on the fly, and the GPUMD ecosystem. After presenting these functionalities, we review a range of applications enabled by GPUMD, particularly in combination with the NEP approach. Finally, we outline possible future development directions for GPUMD.

## KEYWORDS

GPUMD, interatomic potential, machine-learned potential, materials simulation, molecular dynamics

This is an open access article under the terms of the Creative Commons Attribution License, which permits use, distribution and reproduction in any medium, provided the original work is properly cited.

© 2025 The Author(s). *Materials Genome Engineering Advances* published by Wiley-VCH GmbH on behalf of University of Science and Technology Beijing.

## 1 | INTRODUCTION

The molecular dynamics (MD) simulation method is one of the most powerful atomistic simulation methods used to study material properties, ranging from the atomic to the micro and even the mesoscale. An MD package serves as the computational engine behind atomistic simulations, making it an essential tool for researchers in this field. Open-source MD packages play a pivotal role in the development of algorithms and their practical applications. Among the most widely used free and open-source MD packages are GRO-MACS,<sup>[1]</sup> LAMMPS,<sup>[2]</sup> and OpenMM,<sup>[3]</sup> to name a few. The graphics processing units molecular dynamics (GPUMD) package, which also belongs to this group, is the subject of this review. While not yet as widely adopted as the aforementioned packages, GPUMD has been gaining popularity at a rapid pace (Figure 1). It has been included in the list maintained by Talirz et al.,<sup>[4,5]</sup> which tracks trends and statistics in atomistic simulation engines, and exhibits the highest relative growth rate for the last 2 years. Since its first release in August 2017 (version 1.0)<sup>[6]</sup> and the update in May 2022 (version 3.3.1),<sup>[7]</sup> many new features have been added, warranting a comprehensive review.

GPUMD has many distinguishing features making it appealing to both users and developers. It is an MD package developed for heterogeneous CPU-GPU computing platforms from the ground up, like HOOMD-blue<sup>[8]</sup> and GALAMOST<sup>[9]</sup> (later updated to PyGAMD<sup>[10]</sup>). It is also one of the first MD packages that incorporates native machine-learned potentials, which makes it applicable to numerous complex materials that are inaccessible to traditional empirical potentials. The machine-learned potentials in GPUMD can deliver near-quantum-mechanical accuracy at the speed of empirical potentials, enabling predictive and

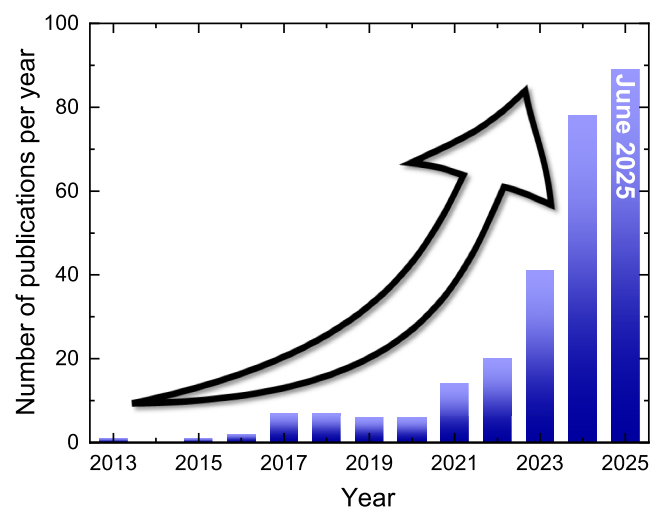


**FIGURE 1** Number of publications (including preprints) per year using graphics processing units molecular dynamics, up to June 14, 2025.

efficient simulations of a wide range of processes and properties. In this paper, we give a comprehensive review and discussion of the past, present, and future of GPUMD.

## 2 | THE DEVELOPMENT HISTORY OF GPUMD

Although the first version of GPUMD was released in 2017,<sup>[6]</sup> its development dates back to 2011 when it began as an exercise for a CUDA programming course. At that time, the package only supported the Lennard-Jones potential and its sole functionality was to calculate the thermal conductivity via the Green–Kubo method. This functionality was further developed in 2013, with improved computational efficiency for the Coulomb-Buckingham potential.<sup>[11]</sup>

In 2015, a general formulation of force, virial, and heat current for many-body potentials was developed, providing the foundation for an efficient implementation of the heat current.<sup>[12]</sup> This advancement led to an efficient GPU implementation<sup>[6]</sup> of many-body potentials such as the embedded atom method,<sup>[13,14]</sup> Stillinger–Weber,<sup>[15]</sup> and Tersoff potentials.<sup>[16]</sup> With these developments, the first version of GPUMD<sup>[6]</sup> was released as an open-source software in 2017, containing about 10,000 lines of source code, written in CUDA C.

The next major development in GPUMD was the addition of the homogeneous nonequilibrium MD method<sup>[17]</sup> and related spectral decomposition techniques<sup>[17–19]</sup> during 2018 and 2019. These developments made GPUMD a popular package for heat transport applications.

In 2019, the development of interatomic potentials, such as a variant of the Tersoff potential<sup>[20]</sup> and the so-called force-constant potential,<sup>[21]</sup> began. However, the focus quickly shifted to general-purpose machine-learned potentials. In 2021, a native machine-learned potential, the neuroevolution potential (NEP),<sup>[22]</sup> was developed. The NEP approach underwent several improvements<sup>[7,23,24]</sup> from 2021 to 2024. The rapid growth in the popularity of GPUMD in recent years has been driven to a large extent by the development of the NEP approach, which provides highly efficient and accurate potential models for a wide range of materials.<sup>[25]</sup>

The latest version of GPUMD, released<sup>[26]</sup> in April 2025, is GPUMD 4.0, which we will describe here. It contains about 85,000 lines of source code written in CUDA C++. For simplicity, we will use GPUMD to refer to GPUMD 4.0 unless otherwise stated.

## 3 | CURRENT FEATURES IN GPUMD

We categorize the functionalities of GPUMD into three major areas: potentials, integrators, and properties. For a detailed discussion on CUDA programming aspects and the

physical foundations underlying GPUMD, we refer the interested reader to relevant textbooks.<sup>[27,28]</sup> Before examining the three functional categories, we provide a concise overview of GPUMD, focusing on its practical usage.

GPUMD is primarily developed using CUDA C++ (although it has also been adapted to work with HIP). Upon compilation, two executables are generated: `gpumd` and `nep`. The `nep` executable serves the training of NEP models, whereas the `gpumd` executable is designed for conducting MD simulations. For the `nep` executable, two files are required:

1. `nep.in`: This file governs the training process.
2. `train.xyz`: This file contains the training data.

1. `run.in`: This file controls the MD simulation.
2. `model.xyz`: This file defines the system to be simulated.

Similarly, for the `gpumd` executable, at least two files must be provided:

Both the `train.xyz` and `model.xyz` files adhere to the standard extended XYZ file format. The `nep.in` file includes straightforward commands that specify the hyperparameters for NEP training.

In contrast, the `run.in` file is comparatively more complex and flexible. In the simplest cases, users only need to define the interatomic potential using the potential keyword and create `ensemble-run` blocks to specify the MD simulation process. Within an `ensemble-run` block, users can incorporate operations to modify the simulation process or compute and output useful quantities. More details will be discussed later, and comprehensive documentation is available at <https://gpumd.org/>.

### 3.1 | Interatomic potentials

Interatomic potentials describe the interactions between atoms and are required inputs to MD simulations. GPUMD supports both conventional empirical potentials and machine-learned potentials, as listed in Table 1.

#### 3.1.1 | Empirical potentials

With respect to empirical potentials, GPUMD supports the 12-6 Lennard-Jones potential,<sup>[29]</sup> the embedded atom method potential,<sup>[13,14]</sup> the Tersoff potential,<sup>[16]</sup> and the registry-dependent interlayer potential.<sup>[33–36]</sup> The interlayer potential accurately describes anisotropic interlayer van der Waals interactions of layered materials and is usually used in combination with another potential for the intralayer interactions. Note that the NEP approach has been specifically implemented<sup>[31]</sup> as an intralayer potential that retains the computational efficiency of traditional empirical potentials such as Tersoff while achieving near ab initio accuracy.

#### 3.1.2 | Machine-learned potentials

For machine-learned potentials, GPUMD currently supports three types: the force-constant potential,<sup>[21]</sup> the NEP, and the deep potential.<sup>[30]</sup> Both force constant and deep potential models need to be trained using external packages, specifically the `hiphive`<sup>[37]</sup> and `DeePMD-kit`<sup>[30]</sup> packages, respectively. The NEP approach, on the other hand, is a native machine-learned potential fully implemented in GPUMD, including both training and inference.

#### 3.1.3 | Formulation of force, virial, and heat current

For all the interatomic potentials in GPUMD, the implementation follows the formalism established for general many-body potentials.<sup>[12]</sup> All the potential models are defined in terms of the site energy  $U_i$  for a given atom  $i$ , whose summation gives the total potential energy of the system:

$$U = \sum_i U_i.$$

The site energy generally depends on its local environment and can be formally expressed as

TABLE 1 Interatomic potentials implemented in the graphics processing units molecular dynamics package.

Interatomic potential	Reference	Comments
Lennard-Jones (LJ)	[29]	The classical two-body potential
Embedded-atom method (EAM)	[13, 14]	Empirical many-body potential for metals
Tersoff	[16]	Empirical many-body potential for covalent bonds
Force-constant potential (FCP)	[21]	Machine-learned potential for equilibrium dynamics
Neuroevolution potential (NEP)	[7, 22–24]	General-purpose machine-learned potential
Deep potential (DP)	[30]	General-purpose machine-learned potential
Hybrid anisotropic interlayer potential (ILP) and NEP	[31]	For various Van der Waals structures
Hybrid ILP and Stillinger–Weber (SW) potential	[32]	For transition metal dichalcogenide structures

$$U_i = U_i(\{\mathbf{r}_{ij}\}_{j \in \mathcal{N}_i}),$$

where  $\{\mathbf{r}_{ij}\}_{j \in \mathcal{N}_i}$  is the set of position differences from atom  $i$  to neighboring atoms  $j \in \mathcal{N}_i$ :

$$\mathbf{r}_{ij} \equiv \mathbf{r}_j - \mathbf{r}_i.$$

The force acting on atom  $i$  can be derived as follows:

$$\begin{aligned} \mathbf{F}_i &= -\frac{\partial}{\partial \mathbf{r}_i} \sum_j U_j \\ &= -\frac{\partial U_i}{\partial \mathbf{r}_i} - \frac{\partial}{\partial \mathbf{r}_i} \sum_{j \neq i} U_j \\ &= -\sum_{j \neq i} \frac{\partial U_i}{\partial \mathbf{r}_{ij}} \frac{\partial \mathbf{r}_{ij}}{\partial \mathbf{r}_i} - \sum_{j \neq i} \sum_{k \neq j} \frac{\partial U_j}{\partial \mathbf{r}_{jk}} \frac{\partial \mathbf{r}_{jk}}{\partial \mathbf{r}_i} \\ &= \sum_{j \neq i} \frac{\partial U_i}{\partial \mathbf{r}_{ij}} - \sum_{j \neq i} \frac{\partial U_j}{\partial \mathbf{r}_{ji}} \\ &= \sum_{j \neq i} \left( \frac{\partial U_i}{\partial \mathbf{r}_{ij}} - \frac{\partial U_j}{\partial \mathbf{r}_{ji}} \right). \end{aligned}$$

This establishes the validity of the (weak form of) Newton's third law. That is, for a general many-body potential, there exists a pair-wise force

$$\mathbf{F}_{ij} = \frac{\partial U_i}{\partial \mathbf{r}_{ij}} - \frac{\partial U_j}{\partial \mathbf{r}_{ji}} \quad (1)$$

between any pair of atoms  $i$  and  $j$  that fulfills

$$\mathbf{F}_{ij} = -\mathbf{F}_{ji}.$$

After realizing the existence of the above pairwise force, the virial tensor and heat current can be elegantly formulated. Starting from the definition of the virial tensor, we have

$$\begin{aligned} \mathbf{W} &\equiv \sum_i \mathbf{r}_i \otimes \mathbf{F}_i \\ &= \sum_i \sum_{j \neq i} \mathbf{r}_i \otimes \mathbf{F}_{ij} \\ &= \sum_i \sum_{j \neq i} \mathbf{r}_i \otimes \left( \frac{\partial U_i}{\partial \mathbf{r}_{ij}} - \frac{\partial U_j}{\partial \mathbf{r}_{ji}} \right) \\ &= \sum_i \sum_{j \neq i} \mathbf{r}_i \otimes \frac{\partial U_i}{\partial \mathbf{r}_{ij}} - \sum_i \sum_{j \neq i} \mathbf{r}_i \otimes \frac{\partial U_j}{\partial \mathbf{r}_{ji}} \\ &= \sum_j \sum_{i \neq j} \mathbf{r}_j \otimes \frac{\partial U_j}{\partial \mathbf{r}_{ji}} - \sum_i \sum_{j \neq i} \mathbf{r}_i \otimes \frac{\partial U_j}{\partial \mathbf{r}_{ji}} \\ &= \sum_i \sum_{j \neq i} \mathbf{r}_{ij} \otimes \frac{\partial U_j}{\partial \mathbf{r}_{ji}}. \end{aligned} \quad (2)$$

There are a few equivalent expressions for the virial tensor. For example, it can also be expressed as

$$\mathbf{W} = -\sum_i \sum_{j \neq i} \mathbf{r}_{ij} \otimes \frac{\partial U_i}{\partial \mathbf{r}_{ij}}.$$

However, the expression in the last line of Equation (2) is more convenient in heat transport applications. To see this, we derive the heat current from its definition:

$$\mathbf{J} \equiv \frac{d}{dt} \sum_i \mathbf{r}_i \left( U_i + \frac{1}{2} m_i \mathbf{v}_i^2 \right) = \mathbf{J}^{\text{pot}} + \mathbf{J}^{\text{kin}},$$

where  $\mathbf{J}^{\text{kin}} = \sum_i \mathbf{v}_i (U_i + \frac{1}{2} m_i \mathbf{v}_i^2)$  is the kinetic part of the heat current. The potential part can be further derived as follows:

$$\begin{aligned} \mathbf{J}^{\text{pot}} &= \sum_i \mathbf{r}_i \frac{d}{dt} \left( U_i + \frac{1}{2} m_i \mathbf{v}_i^2 \right) \\ &= \sum_i \mathbf{r}_i \left[ \sum_{j \neq i} \frac{\partial U_i}{\partial \mathbf{r}_{ij}} \cdot (\mathbf{v}_j - \mathbf{v}_i) + \mathbf{F}_i \cdot \mathbf{v}_i \right] \\ &= \sum_i \mathbf{r}_i \sum_{j \neq i} \left[ \frac{\partial U_i}{\partial \mathbf{r}_{ij}} \cdot (\mathbf{v}_j - \mathbf{v}_i) + \left( \frac{\partial U_i}{\partial \mathbf{r}_{ij}} - \frac{\partial U_j}{\partial \mathbf{r}_{ji}} \right) \cdot \mathbf{v}_i \right] \\ &= \sum_i \mathbf{r}_i \sum_{j \neq i} \left[ \frac{\partial U_i}{\partial \mathbf{r}_{ij}} \cdot \mathbf{v}_j - \frac{\partial U_j}{\partial \mathbf{r}_{ji}} \cdot \mathbf{v}_i \right] \\ &= -\frac{1}{2} \sum_i \sum_{j \neq i} \mathbf{r}_{ij} \left[ \frac{\partial U_i}{\partial \mathbf{r}_{ij}} \cdot \mathbf{v}_j - \frac{\partial U_j}{\partial \mathbf{r}_{ji}} \cdot \mathbf{v}_i \right] \\ &= -\sum_i \sum_{j \neq i} \mathbf{r}_{ij} \frac{\partial U_i}{\partial \mathbf{r}_{ij}} \cdot \mathbf{v}_j \\ &= \sum_i \sum_{j \neq i} \mathbf{r}_{ij} \frac{\partial U_j}{\partial \mathbf{r}_{ji}} \cdot \mathbf{v}_i. \end{aligned} \quad (3)$$

The last three lines in Equation (3) are all legitimate expressions of the heat current in periodic systems. The last line is, however, a more convenient one in practical implementation, as it only involves the velocity  $\mathbf{v}_i$  of the central atom  $i$ , and not the velocities  $\mathbf{v}_j$  of the neighboring atoms  $j$ . Based on this consideration, we define a per-atom virial according to Equation (2):

$$\mathbf{W}_i = \sum_{j \neq i} \mathbf{r}_{ij} \otimes \frac{\partial U_j}{\partial \mathbf{r}_{ji}} \quad (4)$$

such that  $\mathbf{W} = \sum_i \mathbf{W}_i$  and

$$\mathbf{J}^{\text{pot}} = \sum_i \mathbf{W}_i \cdot \mathbf{v}_i. \quad (5)$$

Therefore, the per-atom virial expression in Equation (4) is the basis for both pressure and heat current calculations in GPUMD.

From Equations (1) and (4), it is evident that the terms  $\partial U_i / \partial \mathbf{r}_{ij}$  and  $\partial U_j / \partial \mathbf{r}_{ji}$  are crucial in these calculations. The term  $\partial U_i / \partial \mathbf{r}_{ij}$  is known as the partial force,<sup>[12]</sup> and the other term can be obtained by exchanging indices ( $i \leftrightarrow j$ ). Thus, the calculations of force, virial (pressure), and heat current in GPUMD ultimately hinge on the calculation of partial forces. This elegant formulation is fundamental for the efficient GPU implementation of many-body potentials without resorting to atomic functions.<sup>[6]</sup>

It is worth emphasizing that the formulation above applies to all potential models in GPUMD. Given that NEP is the most commonly used potential model in GPUMD, we discuss its formulation in more detail below.

### 3.1.4 | Neuroevolution potentials

The NEP approach generally follows the Behler–Parinello neural network potential methodology,<sup>[38]</sup> but it differs in terms of the atomic-environment descriptor and the training method. Specifically, we describe the latest version of NEP here, known as NEP4.<sup>[24]</sup>

In NEP4, the site energy  $U_i$  for a given atom  $i$  is a function of an abstract descriptor vector  $\mathbf{q}^i$  with a number of components  $q_v^i$  ( $v = 1, 2, \dots, N_{\text{des}}$ ). Each descriptor component characterizes the structural and chemical environments of atom  $i$  partially. The descriptor components are divided into two groups, one with radial dependence only, called radial descriptors, and the other with additional angular dependence, called angular descriptors.

The radial descriptors are labeled by the index  $n$  and are constructed as a sum of radial functions over the neighboring atoms:

$$q_n^i = \sum_{j \neq i} g_n(r_{ij}). \quad (6)$$

The radial function  $g_n(r_{ij})$  is constructed as a linear combination of a set of  $N_{\text{bas}}^R + 1$  basis functions:

$$g_n(r_{ij}) = \sum_{k=0}^{N_{\text{bas}}^R} c_{nk}^{IJ} f_k(r_{ij}). \quad (7)$$

The basis functions  $f_k(r_{ij})$  are defined as

$$f_k(r_{ij}) = \frac{1}{2} \left[ T_k \left( 2(r_{ij}/r_c^R - 1)^2 - 1 \right) + 1 \right] f_c(r_{ij}),$$

where  $T_k(x)$  is the  $k$ -th order Chebyshev polynomial of the first kind. The function  $f_c(r_{ij})$  is a smoothing function defined as

$$f_c(r_{ij}) = \begin{cases} \frac{1}{2} [1 + \cos(\pi r_{ij}/r_c^R)], & r_{ij} \leq r_c^R; \\ 0, & r_{ij} > r_c^R, \end{cases}$$

where  $r_c^R$  is a cutoff radius beyond which the basis functions are zero. The chemical species are embedded in the expansion coefficients  $c_{nk}^{IJ}$  of the radial functions, where  $I$  and  $J$  indicate the types of atoms  $i$  and  $j$ . These coefficients are trainable, resulting in different radial functions for different pairs of atoms.

The angular descriptors depend both on the radial distances  $r_{ij}$ , and the angles  $\theta_{ijk}$  formed by the  $\mathbf{r}_{ij}$  and  $\mathbf{r}_{ik}$  vectors,

$$\cos \theta_{ijk} = \frac{\mathbf{r}_{ij} \cdot \mathbf{r}_{ik}}{r_{ij} r_{ik}}.$$

The simplest angular descriptors in NEP are defined in terms of the Legendre polynomials  $P_l(x)$ :

$$q_{nl}^i = \frac{2l+1}{4\pi} \sum_{j \neq i} \sum_{k \neq i} g_n(r_{ij}) g_n(r_{ik}) P_l(\cos \theta_{ijk}). \quad (8)$$

The radial and angular dependencies are indicated by the subscripts  $n$  and  $l$  in  $q_{nl}^i$ . Note that the radial functions in  $q_{nl}^i$  are defined similarly to Equation (7) but a different cutoff radius  $r_c^A$  and expansion order  $N_{\text{bas}}^A$  can be used. Efficient evaluation of the angular descriptors requires transforming the Legendre polynomial to spherical harmonics. There are also other types of angular descriptors in NEP. For more details, we refer to ref. [7].

The descriptor vector  $\mathbf{q}^i$  is assembled from the radial and angular descriptors described above. Then, the site energy in NEP is formally written as  $U_i(\mathbf{q}^i)$ . Currently, only a single hidden layer is used in the neural network model for NEP, and the site energy can be explicitly written as

$$U_i = \sum_{\mu=1}^{N_{\text{neu}}} w_{\mu}^{(1)} \tanh \left( \sum_{v=1}^{N_{\text{des}}} w_{\mu v}^{(0)} q_v^i - b_{\mu}^{(0)} \right) - b^{(1)}. \quad (9)$$

Here,  $\tanh(x)$  is the activation function,  $w^{(0)}$  are the weight parameters connecting the input layer (with dimension  $N_{\text{des}}$ ) and the hidden layer (with dimension  $N_{\text{neu}}$ ),  $w^{(1)}$  represents the weight parameters connecting the hidden layer and the output layer (the site energy),  $b^{(0)}$  represents the bias parameters in the hidden layer, and  $b^{(1)}$  is the bias parameter in the output layer. All these parameters are trainable, similar to the expansion coefficients in the radial functions.

In terms of the descriptor vector, the partial force can be written as

$$\frac{\partial U_i}{\partial \mathbf{r}_{ij}} = \sum_{v=1}^{N_{\text{des}}} \frac{\partial U_i}{\partial q_v^i} \frac{\partial q_v^i}{\partial \mathbf{r}_{ij}}$$

With the partial force available, force, virial, and heat current can all be readily evaluated. The derivative  $\partial q_v^i / \partial \mathbf{r}_{ij}$  could be evaluated using auto-differentiation techniques. However, we opted to derive explicit and simplified expressions by hand and implemented them using native CUDA kernels. This approach reduces external dependencies of the GPUMD package and optimizes its computational performance.

NEP can be used in combination with other potentials.<sup>[39,40]</sup> In addition to the interlayer potential mentioned above, it can also be used in combination with the DFT-D3 potential<sup>[41]</sup> and the Ziegler-Biersack-Littmark potential.<sup>[42]</sup> The DFT-D3 potential can capture weak van der Waals interactions, whereas the Ziegler-Biersack-Littmark potential is usually used to ensure the physicality of the (repulsive) interaction when atoms get very close to each other.

Recently, Liang et al.<sup>[43]</sup> developed NEP89, a comprehensive foundation model covering virtually the entire periodic table, which has been released alongside GPUMD 4.0. NEP89 can be used out of the box or as a starting point that can be conveniently fine-tuned with a relatively small amount of additional training data for system-specific applications. NEP89 achieves competitive accuracy compared to representative foundation models across a range of properties, including energetics, elastic properties, phonon frequencies, and MD simulations of amorphous carbon, liquid water, and solid-state electrolytes, while being three to four orders of magnitude more computationally efficient, enabling large-scale atomistic simulations of inorganic and organic systems that were previously impractical. The NEP89 model is the first one in a series of NEP-based foundation models, which are expected to exhibit better capabilities in future versions.

The NEP approach, as implemented in GPUMD, achieves exceptionally high computational performance. Using a single GPU, either professional or consumer grade, NEP-GPUMD can achieve a computational speed of the order of  $10^7$  atom-step per second in typical MD simulations. The number of atoms in the simulation cell manageable with a single GPU ranges from 1 to 10 million, depending on the device memory of the GPU. With eight 80-GB A100 GPUs, NEP has been used to simulate a high-entropy alloy with 100 million atoms.<sup>[24]</sup> The outstanding computational performance advantage of NEP over other representative GPU-based machine-learned potentials, such as deep potential (DP),<sup>[30]</sup> NequIP,<sup>[44]</sup> and MACE,<sup>[45]</sup> is clearly demonstrated in Table 2.

## 3.2 | Integrators and related operations

### 3.2.1 | The velocity-Verlet integrator

Integrators solve the equations of motion and are central to the atomic dynamics in MD simulations. Without any external control, an isolated system adheres to Hamiltonian dynamics,

**TABLE 2** Computational speed (in units of atom-step per second per GPU) of neuroevolution potential (NEP) (within graphics processing units molecular dynamics) compared to representative GPU-based machine-learned potentials (MLPs), including deep potential (DP),<sup>[30]</sup> NequIP,<sup>[44]</sup> and MACE,<sup>[45]</sup> all interfaced to LAMMPS.<sup>[2]</sup>

Material	Speed	MLP	GPU	Reference
2D Silicene	870,000	DP	V100	[22]
	13,000,000	NEP	V100	[22]
Bulk PbTe	520,000	DP	V100	[22]
	11,000,000	NEP	V100	[22]
Tungsten	130,000	DP	A100	[39]
	13,000,000	NEP	A100	[39]
Diamond	1200	MACE	V100	[25]
	2000	NequIP	V100	[25]
	1,830,000	NEP	V100	[25]

resulting in a microcanonical ensemble. In this ensemble, the number of particles  $N$ , the volume  $V$  (or more precisely the simulation cell), and the total energy  $E$  of the system remain constant. Hence, it is known as the  $NVE$  ensemble. The velocity-Verlet integrator<sup>[46]</sup> is used in GPUMD, which can be formulated more formally in terms of the Liouville operator and the Trotter decomposition.<sup>[47]</sup> The integration for one time step  $\Delta t$  can be expressed as follows:

$$\mathbf{r}_i(t + \Delta t) \approx \mathbf{r}_i(t) + \mathbf{v}_i(t)\Delta t + \frac{1}{2} \frac{\mathbf{F}_i(t)}{m_i} (\Delta t)^2;$$

$$\mathbf{v}_i(t + \Delta t) \approx \mathbf{v}_i(t) + \Delta t \frac{\mathbf{F}_i(t) + \mathbf{F}_i(t + \Delta t)}{2m_i}.$$

In GPUMD, a statistical ensemble is specified by the `ensemble` keyword, followed by a specific ensemble type. For example, the  $NVE$  ensemble is invoked by the combined keyword `ensemble nve`. The keywords for the various integrators/ensembles and related operations are listed in Table 3.

### 3.2.2 | Thermostats and barostats

Other statistical ensembles can be realized by controlling temperature  $T$  and/or pressure  $P$ . By controlling the temperature only, we have the  $NVT$  ensemble. Here, the energy is not constant, but the temperature has a well-defined mean value in equilibrium. GPUMD supports several thermostats for temperature control, including the Berendsen thermostat<sup>[48]</sup> (`ensemble nvt_ber`), the Nosé-Hoover chain thermostat<sup>[47]</sup> (`ensemble nvt_nhc`), the Bussi-Donadio-Parrinello thermostat (also called stochastic velocity rescaling thermostat)<sup>[49]</sup> (`ensemble nvt_bdp`), and the Langevin thermostats<sup>[50,51]</sup> (`ensemble nvt_lan` and `ensemble nvt_bao`). By controlling the pressure as well,

TABLE 3 Integrators and related operations implemented in the graphics processing units molecular dynamics package.

Integrators/ensembles	Keyword
NVE	ensemble nve
Berendsen NVT	ensemble nvt_ber
NHC NVT	ensemble nvt_nhc
BDP NVT	ensemble nvt_bdp
Langevin NVT	ensemble nvt_lan
Langevin NVT	ensemble nvt_bao
Berendsen NPT	ensemble npt_ber
SCR NPT	ensemble npt_scr
MTTK NPT	ensemble npt_mttk
MTTK-based NPH	ensemble nph_mttk
NEMD heat transport	ensemble heat_nhc
NEMD heat transport	ensemble heat_bdp
NEMD heat transport	ensemble heat_lan
Equilibrium TI	ensemble ti
Nonequilibrium TI	ensemble ti_spring
Nonequilibrium TI, RS path	ensemble ti_rs
Nonequilibrium TI, AS path	ensemble ti_as
Nonequilibrium TI, liquid	ensemble ti_liquid
Hugoniosat shock method	ensemble nphug
NEMD shock piston	ensemble wall_piston
NEMD shock mirror	ensemble wall_mirror
NEMD shock harmonic	ensemble wall_harmonic
MSST	ensemble msst
PIMD	ensemble pimd
RPMD	ensemble rpmd
TRPMD	ensemble trpmd
Canonical MC	mc canonical
SGC-MC	mc sgc
VCSGC-MC	mc vcsgc
Change box once	change_box
Deform box during a run	deform
Fix a group of atoms	fix
Move a group of atoms	move
Add external forces to atoms	add_force
Add electric field to ions	add_efield
Add stopping forces to atoms	electron_stop

Abbreviations: AS, adiabatic switching; BDP, Bussi-Donadio-Parrinello; MSST, multi-scale shock technique; MTTK, Martyna-Tuckerman-Tobias-Klein; NEMD, nonequilibrium molecular dynamics; NHC, Nose-Hoover chain; PIMD, path-integral molecular dynamics; RPMD, ring-polymer molecular dynamics; RS, reversible scaling; SCR, stochastic cell rescaling; SGC, semi-grand canonical; TI, thermodynamic integration; TRPMD, thermostatted RPMD; VCSGC, variance-constrained SGC.

we have the *NPT* ensemble. GPUMD supports a few barostats for pressure control, including the Berendsen barostat<sup>[48]</sup> (ensemble *npt\_ber*), the Martyna-Tuckerman-Tobias-Klein barostat<sup>[47]</sup> (ensemble *npt\_mttk*), and the Bernetti-Bussi barostat (also called stochastic cell rescaling barostat)<sup>[52]</sup> (ensemble *nvt\_scr*). If pressure is controlled but temperature is not, we have the *NPH* ensemble which conserves the enthalpy *H* in equilibrium. This has only been implemented in the Martyna-Tuckerman-Tobias-Klein approach<sup>[47]</sup> (ensemble *nph\_mttk*).

The thermostats can also be applied locally to a group of atoms to enable nonequilibrium MD simulations for applications such as heat transport. These include the Bussi-Donadio-Parrinello thermostat (ensemble *heat\_bdp*), the Nose-Hoover chain thermostat (ensemble *heat\_nhc*), and the Langevin thermostat (ensemble *heat\_lan*). Among these, the Langevin thermostat is recommended for heat transport applications.<sup>[53]</sup>

### 3.2.3 | Thermodynamic integration and free energy calculations

We have implemented a series of thermodynamic integration methods for Helmholtz and Gibbs free-energy calculations, which are useful for studying phase diagrams. These include the equilibrium approach (ensemble *ti*) and nonequilibrium approach (ensemble *ti\_spring*). These methods only apply to solids, and the free energies are calculated in reference to the Einstein crystal.<sup>[54]</sup> The nonequilibrium approaches allow for efficient integration along a reversible scaling path<sup>[55]</sup> (ensemble *ti\_rs*) or an adiabatic switching path<sup>[56]</sup> (ensemble *ti\_as*). For liquids (ensemble *ti\_liquid*), the free energies are calculated in reference to the Uhlenbeck-Ford model.<sup>[57]</sup>

### 3.2.4 | Shock simulation methods

We have implemented a few shock methods.<sup>[58]</sup> One method is based on the constant stress Hugoniosat method<sup>[59]</sup> (ensemble *nphug*). With a target stress, this algorithm adjusts the temperature to make the system converge to the Hugoniot. Another method is based on the multiscale shock technique<sup>[60]</sup> (ensemble *msst*). Besides, there are a few nonequilibrium MD methods, where a shock wave is generated by a moving wall, which can be a fixed layer of atoms (piston) (ensemble *wall\_piston*), a momentum mirror that reflects atoms (ensemble *wall\_mirror*), or a harmonic potential that pushes atoms away (ensemble *wall\_harmonic*).

### 3.2.5 | Path-integral methods

The above integrators are for classical MD simulations. Nuclear quantum effects can be partially captured by path-

integral MD simulation methods, which have recently been implemented into GPUMD.<sup>[61]</sup> Apart from the normal path-integral MD algorithm based on the Langevin thermostat and normal modes<sup>[60]</sup> (ensemble pimd), we also implemented the ring-polymer MD<sup>[62]</sup> (ensemble rpmd) and thermostatted ring-polymer MD<sup>[63]</sup> (ensemble trpmd). For the normal modes, we used the robust integration algorithm based on the Cayley transform.<sup>[64]</sup>

### 3.2.6 | Hybrid Monte Carlo and molecular dynamics

MD simulations can be supplemented by Monte Carlo simulations to enable sampling of the compositional degrees of freedom in mixed (alloyed) systems. Recently, a series of hybrid Monte Carlo and MD simulation methods has been implemented into GPUMD,<sup>[65]</sup> including the canonical Monte Carlo ensemble (exchanging pairs of atoms of different species) (mc canonical), the semi-grand canonical Monte Carlo ensemble (flipping the species of single atoms) (mc sgc), and the variance-constrained semi-grand canonical Monte Carlo ensemble<sup>[66,67]</sup> (mc vcsgc). The choice of input parameters in terms of normalization follows the expressions in ref. [68].

### 3.2.7 | Other operations

Apart from the various integrators/ensembles, the time evolution can also be altered by other related operations. The `change_box` keyword can be used to deform the box instantly, and the `deform` keyword can be used to deform the box during a run. A group of atoms can be fixed (frozen) by using the `fix` keyword or be moved as a rigid body using the `move` keyword. External forces can be added to the atoms via the `add_force` keyword, and external electric forces can be added to ions (charged atoms) via the `add_efield` keyword. Frictional forces on fast-moving atoms due to electronic collisions can be invoked by the `electron_stop` keyword, which is useful in irradiation damage or ion implantation simulations.

## 3.3 | Properties

The usefulness of a MD package is finally manifested in the physical properties that can be calculated using it. GPUMD supports dumping of trajectories and moreover enables the calculation of many useful quantities on the fly (Table 4).

### 3.3.1 | The dump-like keywords

During any MD simulation, it is recommended to dump the basic thermodynamic quantities for the whole system, using

**TABLE 4** Dump and compute keywords implemented in the graphics processing units molecular dynamics package.

Properties	Keyword
Thermodynamic quantities	<code>dump_thermo</code>
Trajectory and related quantities	<code>dump_xyz</code>
Trajectory for the beads in PIMD	<code>dump_beads</code>
Restarting file	<code>dump_restart</code>
Space–time average	<code>compute</code>
RDF	<code>compute_rdf</code>
ADF	<code>compute_adf</code>
Angular-dependent RDF	<code>compute_angular_rdf</code>
SDC	<code>compute_sdc</code>
MSD	<code>compute_msd</code>
Viscosity	<code>compute_viscosity</code>
EMD thermal transport	<code>compute_hac</code>
HNEMD thermal transport	<code>compute_hnemd</code>
HNEMDEC thermal transport	<code>compute_hnemdec</code>
Spectral decomposition	<code>compute_shc</code>
Modal decomposition (EMD)	<code>compute_gkma</code>
Modal decomposition (HNEMD)	<code>compute_hnema</code>
Electronic transport	<code>compute_lsqt</code>
Phonon properties	<code>compute_phonon</code>
VDOS	<code>compute_dos</code>

Abbreviations: ADF, angular distribution function; EMD, equilibrium molecular dynamics; HNEMD, homogeneous nonequilibrium molecular dynamics; HNEMDEC, HNEMD with Evans-Cummings algorithm; MSD, mean-square displacement; RDF, radial distribution function; RPMD, ring-polymer molecular dynamics; SDC, self-diffusion coefficient; VDOS, vibrational density of states.

the `dump_thermo` keyword. The quantities dumped include temperature, kinetic energy, potential energy, pressure tensor, and the simulation cell metric.

Trajectories and related quantities can be dumped using the `dump_xyz` keyword. This will generate an output file in the extended XYZ format that can be visualized by programs such as OVITO.<sup>[69]</sup> In this file, the trajectory is stored frame by frame. Each frame contains  $N + 2$  lines, where  $N$  is the number of atoms in the frame that is written in the first line. The second line contains information such as the global time, boundary conditions, cell metric, total energy, virial, and stress. The next  $N$  lines then contain the atom symbols, positions, and possibly other per-atom quantities. A related keyword for path-integral MD simulations is `dump_beads`. Finally, the `dump_restart` keyword can be used to save a file that can be used to restart a simulation, although the present implementation does not lead to a perfect restart in some cases, such as those involving the Nosé–Hoover chain thermostat, where some thermostating variables are not saved in the restart file. This is expected to be improved during the next code refactoring process.

### 3.3.2 | The compute-like keywords

The compute-like keywords are used to calculate physical quantities on the fly. The simplest keyword is `compute`, which calculates the spatial and time averages of various quantities. This is useful for, for example, getting a temperature profile or a stress distribution. There are also keywords for common structural properties, such as the radial distribution function (`compute_rdf`), the angular distribution function (`compute_adf`), and the angular-dependent radial distribution function (`compute_ardf`).

The majority of the compute-like keywords are related to transport properties. These usually involve time-correlation functions, making on-the-fly calculations valuable for minimizing data storage. The transport properties include the self-diffusion coefficient from the velocity autocorrelation function (`compute_sdc`) or the mean-square displacement (`compute_msd`), the viscosity (`compute_viscosity`), the thermal conductivity from heat current autocorrelation function (`compute_hac`), the thermal conductivity from homogeneous nonequilibrium MD simulations<sup>[17]</sup> (`compute_hnemd` and `compute_hnemdec`), the spectral (`compute_shc`)<sup>[17]</sup> and modal<sup>[19]</sup> (`compute_hnema` and `compute_gkma`) decompositions as well as electronic transport properties from the linear-scaling quantum transport methods<sup>[70]</sup> (`compute_lsqt`). The linear-scaling quantum transport calculations are based on tight-binding models.

GPUMD also supports the direct calculation of phonon properties, such as phonon dispersions using the finite-displacement method (`compute_phonon`) and vibrational density of states from the mass-weighted velocity autocorrelation function (`compute_vdos`).

## 4 | THE GPUMD ECOSYSTEM

Although the `nep` and `gpumd` executables are standalone programs that operate without external dependencies, they can be complemented by other tools and packages, collectively forming the GPUMD ecosystem.

### 4.1 | Tools within the GPUMD package

The tools are included with the `tools` directory of the GPUMD package. Most utilities in the `tools` directory focus on the preparation and analysis of training and test datasets for NEP. For example, `abacus2xyz`, `castep2xyz`, `cp2k2xyz`, `orca2xyz`, and `vasp2xyz` are designed to convert outputs from various quantum chemistry packages into training/test datasets formatted in the extended XYZ format. Similarly, `dp2xyz`, `mtp2xyz`, and `runner2xyz` facilitate the conversion of training datasets from other formats into the extended XYZ format.

### 4.2 | Additional related packages

Additional related packages are listed in Table 5, most of which are based on the `NEP_CPU` package. This package contains a standalone C++ implementation of the inference of NEP, which serves as the computational engine for many Python-based packages listed in Table 5. Furthermore, it provides an interface to the LAMMPS package,<sup>[2]</sup> enabling NEP to function in more computing environments.

The `calorine` package<sup>[71]</sup> is a versatile Python library designed to construct and use NEP models, offering ASE (Atomic Simulation Environment)<sup>[79]</sup> calculators, input/output functions for GPUMD files, NEP model inspection, descriptor space analysis, structure generation, and NEP training, and can be easily used to perform various calculations, including relaxation, phonon properties, elastic properties, free energy calculations, thermal conductivity via the Boltzmann transport equation, and so on.

The `dynasor` package<sup>[72,73]</sup> is designed for calculating total and partial dynamic structure factors as well as related correlation functions from MD simulations, including particularly those driven by GPUMD. By analyzing these functions, one can access the dynamics of a system without resorting to perturbative approaches. It can also predict

TABLE 5 Packages and repositories related to graphics processing units molecular dynamics (GPUMD) and/or neuroevolution potential (NEP).

Packages	Code repository
NEP_CPU	<a href="https://github.com/brucefan1983/NEP_CPU">https://github.com/brucefan1983/NEP_CPU</a>
calorine <sup>[71]</sup>	<a href="https://gitlab.com/materials-modeling/calorine">https://gitlab.com/materials-modeling/calorine</a>
dynasor <sup>[72,73]</sup>	<a href="https://gitlab.com/materials-modeling/dynasor">https://gitlab.com/materials-modeling/dynasor</a>
GPUMD-Wizard	<a href="https://github.com/Jonsnow-willow/GPUMD-Wizard">https://github.com/Jonsnow-willow/GPUMD-Wizard</a>
Gpyumd	<a href="https://github.com/AlexGabourie/gpyumd">https://github.com/AlexGabourie/gpyumd</a>
GPUMDkit	<a href="https://github.com/zhyan0603/GPUMDkit">https://github.com/zhyan0603/GPUMDkit</a>
MAGUS <sup>[74,75]</sup>	<a href="https://gitlab.com/bigd4/magus">https://gitlab.com/bigd4/magus</a>
mdapy <sup>[76]</sup>	<a href="https://github.com/mushroomfire/mdapy">https://github.com/mushroomfire/mdapy</a>
NepTrain <sup>[77]</sup>	<a href="https://github.com/aboys-cb/NepTrain">https://github.com/aboys-cb/NepTrain</a>
NepTrainKit <sup>[77]</sup>	<a href="https://github.com/aboys-cb/NepTrainKit">https://github.com/aboys-cb/NepTrainKit</a>
NEP_Active	<a href="https://github.com/psn417/NEP_Active">https://github.com/psn417/NEP_Active</a>
nep_maker	<a href="https://github.com/psn417/nep_maker">https://github.com/psn417/nep_maker</a>
PyNEP	<a href="https://github.com/bigd4/PyNEP">https://github.com/bigd4/PyNEP</a>
PySED <sup>[78]</sup>	<a href="https://github.com/Tingliangstu/pySED">https://github.com/Tingliangstu/pySED</a>
Somd	<a href="https://github.com/initqp/somd">https://github.com/initqp/somd</a>
nep-data	<a href="https://gitlab.com/brucefan1983/nep-data">https://gitlab.com/brucefan1983/nep-data</a>
GPUMD-Tutorials	<a href="https://github.com/brucefan1983/GPUMD-Tutorials">https://github.com/brucefan1983/GPUMD-Tutorials</a>

experimental spectra by combining the structure factor with the cross sections or form factors.

GPUMD-Wizard, a material structure processing software based on ASE, automates the calculation of various material properties, including lattice constants, elastic constants, and defect formation energies, while also facilitating the execution and analysis of MD simulations using GPUMD.

The `gpyumd` package is a collection of tools that generate valid input files and process the output files of GPUMD. It leverages the functionality of ASE when beneficial, but is otherwise independent to remain flexible and best serve GPUMD directly.

The MAGUS package<sup>[74,75]</sup> is a machine learning and graph theory assisted crystal structure prediction package. It has interfaces for various quantum chemistry packages and machine-learned potentials, including NEP.

GPUMDkit, a shell-based toolkit for the GPUMD and NEP, offers a user-friendly command-line interface to streamline common scripts and workflows, simplifying tasks such as script invocation, format conversion, structure sampling, NEP construction workflow, and various analyses, aiming to improve user productivity.

The `mdapy`<sup>[76]</sup> Python library provides an array of powerful, flexible, and straightforward tools to analyze atomic trajectories generated from MD simulations. It well supports the extended XYZ format output by GPUMD and takes advantage of the highly parallel processing capabilities on multicore CPUs and GPUs to provide excellent efficiency and flexibility for processing and analyzing trajectories.

`NepTrain` and `NepTrainKit` are Python packages designed to enhance the construction of NEP models, with `NepTrain` integrating tools for active learning workflows, including structural perturbations, configurational space exploration, single-point energy calculations, and force field training, whereas `NepTrainKit` provides user-friendly visualization and processing of NEP training datasets, enabling detailed analysis of dataset composition and model performance.

`NEP_Active` and `nep_maker` also focus on NEP model construction, with `NEP_Active` employing active learning strategies to automate training set construction and `nep_maker` extending this by incorporating a comprehensive workflow to automate active learning by submitting and monitoring jobs.

`PyNEP` serves as a Python interface for NEP, providing ASE calculators, descriptor calculations for atoms, and phonon calculations, but is particularly noted for its implementation of the farthest point sampling method to select representative structures.

`PySED`<sup>[78]</sup> is a Python-based package built upon the spectral energy density method, designed to analyze specific phonon-mode information from large-scale MD trajectories, enabling convenient calculation of kinetic-energy-weighted phonon dispersions and derivation of phonon lifetimes. It was developed to work with NEP-driven MD simulations.

The `somd` package includes a simple wrapper for the `nep` executable, enabling automatic construction of NEP models through active learning strategies.

Finally, we note that numerous training and test datasets related to NEP have been compiled in the `nep-data` repository, although the collection is not exhaustive. Additionally, the `GPUMD-Tutorials` repository offers a wide range of valuable tutorials and examples, covering various practical aspects of the GPUMD package.

## 5 | APPLICATIONS OF GPUMD TO MATERIALS CALCULATIONS

To date, GPUMD has been utilized in approximately two hundred publications. Table 6 provides a comprehensive list of these publications, highlighting the first authors and the primary materials investigated.

### 5.1 | Applications in early years

Prior to 2022, GPUMD applications focused predominantly on covalently bonded systems, which have traditionally been described using the Tersoff potential. Consequently, the range of materials studied during this period was quite limited, primarily comprising two-dimensional materials such as graphene, hexagonal BN, and MoS<sub>2</sub>. Thermal transport was the main theme of these early investigations.

Building on these materials, significant advancements were made in computational methods for heat transport. These include the unambiguous definition of heat current for general many-body potentials,<sup>[12]</sup> the demonstrated equivalence between equilibrium and nonequilibrium MD methods,<sup>[87]</sup> the development of a general formulation for the homogeneous nonequilibrium MD method along with related spectral decomposition techniques,<sup>[17]</sup> the examination of impact of thermostatting methods on the nonequilibrium MD method,<sup>[53]</sup> and the interpretation of apparent thermal conductivity using the equilibrium MD method.<sup>[106]</sup>

Beyond the methodological progress, GPUMD has also been employed to uncover the physical mechanisms underlying phonon thermal transport in various materials. A particularly noteworthy application involved studying heat transport in multilayer MoS<sub>2</sub>, successfully reproducing the experimentally observed highly anisotropic thermal transport.<sup>[108]</sup>

### 5.2 | Applications with NEP

Since 2022, GPUMD has been employed to study a wider range of materials, thanks to the development of the NEP approach in 2021<sup>[22]</sup> and its improvements in 2022<sup>[7,23]</sup> and 2024.<sup>[24]</sup> Heat transport remained a major application area

TABLE 6 Applications of the graphics processing units molecular dynamics package in various materials.

Year	Publications (major materials)
2013	Fan <sup>[111]</sup> (Ar, PbTe)
2015	Fan <sup>[112]</sup> (Si, C)
2016	Hirvonen <sup>[80]</sup> (C); Mortazavi <sup>[81]</sup> (C)
2017	Azizi <sup>[82]</sup> (C); Fan <sup>[6]</sup> (C); Fan <sup>[118]</sup> (C); Fan <sup>[83]</sup> (C); Fan <sup>[84]</sup> (C); Hirvonen <sup>[85]</sup> (C); Mortazavi <sup>[86]</sup> (C)
2018	Dong <sup>[87]</sup> (Si, C); Dong <sup>[88]</sup> (BN); Fan <sup>[89]</sup> (C); Hirvonen <sup>[90]</sup> (C); Mortazavi <sup>[91]</sup> (CN); Rajabpour <sup>[92]</sup> (C); Xu <sup>[93]</sup> (P)
2019	Fan <sup>[17]</sup> (C, Si); Fan <sup>[20]</sup> (Si); Gu <sup>[94]</sup> (C); Isaeva <sup>[95]</sup> (Si); Li <sup>[53]</sup> (C); Xu <sup>[96]</sup> (MoS <sub>2</sub> )
2020	Bea <sup>[97]</sup> (Si); Dong <sup>[98]</sup> (C); Fu <sup>[99]</sup> (Si); Gabourie <sup>[100]</sup> (MoS <sub>2</sub> ); Wu <sup>[101]</sup> (C); Wu <sup>[102]</sup> (BN)
2021	Barbalinardo <sup>[103]</sup> (C); Chen <sup>[104]</sup> (CFs); Dong <sup>[105]</sup> (C/BN); Dong <sup>[106]</sup> (Si, C); Du <sup>[107]</sup> (C/BN); Fan <sup>[22]</sup> (PbTe, Si); Gabourie <sup>[19]</sup> (HfO <sub>2</sub> , SiO <sub>2</sub> ); Kim <sup>[108]</sup> (MoS <sub>2</sub> ); Lundgren <sup>[109]</sup> (SiGe); So <sup>[110]</sup> (C); Wang <sup>[111]</sup> (C); Wu <sup>[112]</sup> (C/BN); Wu <sup>[113]</sup> (C/BN); Zhang <sup>[114]</sup> (C)
2022	Cheng <sup>[115]</sup> (Si-Ge); Dong <sup>[116]</sup> (Si); Fan <sup>[23]</sup> (PbTe); Fan <sup>[7]</sup> (PbTe, C); Feng <sup>[117]</sup> (C); Gabourie <sup>[118]</sup> (MoS <sub>2</sub> ); Jin <sup>[119]</sup> (Si, Ge); Li <sup>[120]</sup> (Al-Mg); Li <sup>[121]</sup> (Si); Li <sup>[122]</sup> (Si); Liang <sup>[123]</sup> (C); Sha <sup>[124]</sup> (C/BN); Sha <sup>[125]</sup> (CN); Wang <sup>[126]</sup> (Li <sub>6</sub> Al); Wu <sup>[127]</sup> (C, BN) Wu <sup>[128]</sup> (C); Wu <sup>[129]</sup> (C); Xu <sup>[130]</sup> (C); Ying <sup>[131]</sup> (C); Zhou <sup>[132]</sup> (Si)
2023	Bea <sup>[133]</sup> (Si); Cheng <sup>[134]</sup> (PbTe); Cheng <sup>[135]</sup> (C); DeVries <sup>[136]</sup> (MX <sub>2</sub> (M = Mo, W; X = S, Se)); Dong <sup>[137]</sup> (C); Du <sup>[138]</sup> (PH <sub>4</sub> AlBr <sub>4</sub> ); Eriksson <sup>[139]</sup> (C, BN, MoS <sub>2</sub> ); Fransson <sup>[140]</sup> (CsPbBr <sub>3</sub> , MAPbI <sub>3</sub> ); Fransson <sup>[141]</sup> (CsPbBr <sub>3</sub> ); Fransson <sup>[142]</sup> (CsPbX <sub>3</sub> (X = Cl, Br, I)); Li <sup>[143]</sup> (C); Liang <sup>[144]</sup> (SiO <sub>2</sub> ); Liu <sup>[39]</sup> (W); Liu <sup>[145]</sup> (Si/Ge); Lu <sup>[146]</sup> (C); Lu <sup>[147]</sup> (C); Ouyang <sup>[148]</sup> (AgX (X = Cl, Br, I)); Pan <sup>[149]</sup> (MgOH); Rosander <sup>[150]</sup> (BaZrO <sub>3</sub> ); Sha <sup>[151]</sup> (PbTe); Shi <sup>[152]</sup> (C); Shi <sup>[153]</sup> (InGeX <sub>3</sub> (X = S, Se, Te)); Shi <sup>[154]</sup> (CsPbX <sub>3</sub> (X = Cl, Br, I)); Su <sup>[155]</sup> (Cs <sub>2</sub> BiAgBr <sub>6</sub> , Cs <sub>2</sub> BiAgCl <sub>6</sub> ); Sun <sup>[156]</sup> (Ga <sub>2</sub> O <sub>3</sub> ); Wang <sup>[157]</sup> (Si); Wang <sup>[158]</sup> (SrTiO <sub>3</sub> ); Wei <sup>[159]</sup> (C); Wiktor <sup>[160]</sup> (CsMX <sub>3</sub> (M = Sn, Pb and X = Cl, Br, I)); Wu <sup>[161]</sup> (C, BN); Wu <sup>[162]</sup> (C, C <sub>3</sub> N); Xiong <sup>[163]</sup> (C); Xu <sup>[164]</sup> (H <sub>2</sub> O); Yang <sup>[165]</sup> (GaN/C); Ying <sup>[166]</sup> (C); Ying <sup>[40]</sup> (MOF); Ying <sup>[167]</sup> (P); Ying <sup>[168]</sup> (MOF); Zhang <sup>[169]</sup> (HfO <sub>2</sub> ); Zhao <sup>[170]</sup> (Pd-Cu-Ni-P); Zhou <sup>[171]</sup> (Ge-Si, Ge)
2024	Berger <sup>[172]</sup> (MoS <sub>2</sub> , BAs); Berger <sup>[173]</sup> (Amino acids); Berrens <sup>[174]</sup> (H <sub>2</sub> O); Cao <sup>[175]</sup> (PC); Chen <sup>[176]</sup> (C, BN); Chen <sup>[177]</sup> (GeSn); Chen <sup>[178]</sup> (H <sub>2</sub> O); Cheng <sup>[179]</sup> (A <sub>2</sub> SnBr <sub>6</sub> (A=Rb, Cs)); Cheng <sup>[180]</sup> (SiGe); Deng <sup>[181]</sup> (Si); Dong <sup>[182]</sup> (Si); Dong <sup>[183]</sup> (ScAlN); Fan <sup>[184]</sup> (MOF); Fan <sup>[70]</sup> (C); Fang <sup>[185]</sup> (CH); Feng <sup>[186]</sup> (C); Fine <sup>[187]</sup> (Ca <sub>3</sub> CrN <sub>3</sub> H); Folkner <sup>[188]</sup> (Si); Fransson <sup>[189]</sup> (MAPbI <sub>3</sub> ); Fransson <sup>[190]</sup> (BaZrO <sub>3</sub> ); Gabourie <sup>[191]</sup> (Si, SiO <sub>2</sub> , HfO <sub>2</sub> ); Huang <sup>[192]</sup> (C); Huang <sup>[193]</sup> (Mg <sub>3</sub> (Sb, Bi) <sub>2</sub> ); Li <sup>[194]</sup> (Gr); Li <sup>[195]</sup> (C); Li <sup>[196]</sup> (Sb-Te); Li <sup>[197]</sup> (Si); Li <sup>[198]</sup> (C <sub>9</sub> H <sub>4</sub> BO <sub>2</sub> ); Li <sup>[199]</sup> (C); Liu <sup>[200]</sup> (HECs); Lyu <sup>[201]</sup> (PbSe); Muhammed <sup>[202]</sup> (Perovskites); Oliveira <sup>[203]</sup> (Si); Pan <sup>[58]</sup> (SiO <sub>2</sub> ); Pegolo <sup>[204]</sup> (Li <sub>x</sub> Si <sub>1-x</sub> ); Qi <sup>[205]</sup> (AlN, C); Ru <sup>[206]</sup> (PdSe <sub>2</sub> ); Schäfer <sup>[207]</sup> (PTA); Shi <sup>[208]</sup> (BN); So <sup>[209]</sup> (Ga <sub>2</sub> O <sub>3</sub> , BN); So <sup>[210]</sup> (C); Song <sup>[24]</sup> (16 metals); Sonti <sup>[211]</sup> (Zeolite-Confined Gold); Sun <sup>[212]</sup> (Co, Mo, Fe, Ni, Cu); Sun <sup>[213]</sup> (AlN, C); Sun <sup>[214]</sup> (Ga <sub>2</sub> O <sub>3</sub> /C); Tang <sup>[215]</sup> (BN); Tang <sup>[216]</sup> (ScF <sub>3</sub> ); Tian <sup>[217]</sup> (NaCl-CaCl <sub>2</sub> ); Tian <sup>[218]</sup> (H <sub>2</sub> O); Timalsina <sup>[219]</sup> (MgNiCoCuZnO <sub>5</sub> ); Wan <sup>[220]</sup> (C <sub>6</sub> N <sub>7</sub> ); Wang <sup>[221]</sup> (COFs); Wang <sup>[222]</sup> (H <sub>2</sub> O); Wang <sup>[223]</sup> (Si); Wang <sup>[224]</sup> (Ga <sub>2</sub> O <sub>3</sub> ); Wei <sup>[225]</sup> (high-entropy rare-earth monosilicates); Wu <sup>[226]</sup> (C); Wu <sup>[227]</sup> (C); Wu <sup>[228]</sup> (Si, GaAs, C, PbTe); Wu <sup>[229]</sup> (C); Wu <sup>[230]</sup> (C, BN); Xu <sup>[231]</sup> (Perovskite); Xu <sup>[232]</sup> (Perovskite); Yan <sup>[233]</sup> (Li <sub>7</sub> La <sub>3</sub> Zr <sub>2</sub> O <sub>12</sub> ); Yang <sup>[234]</sup> (C); Ying <sup>[235]</sup> (C); Yu <sup>[236]</sup> (C); Yu <sup>[237]</sup> (BN); Yue <sup>[238]</sup> (Si/C); Zeraati <sup>[239]</sup> (La <sub>2</sub> Zr <sub>2</sub> O <sub>7</sub> ); Zhang <sup>[240]</sup> (BiI <sub>3</sub> ); Zhang <sup>[241]</sup> (C); Zhang <sup>[242]</sup> (GeTe); Zhang <sup>[243]</sup> (Alanine dipeptide and acetyl chloride); Zhang <sup>[244]</sup> (Li-Be); Zhao <sup>[245]</sup> (Ti-Al-Nb); Zhou <sup>[246]</sup> (LiH)
2025	Ariana <sup>[247]</sup> (Na <sub>3</sub> SbSe <sub>4</sub> ); Bao <sup>[248]</sup> (LiNbO <sub>3</sub> /LN); Berger <sup>[73]</sup> (Ni <sub>3</sub> Al, BaZrO <sub>3</sub> ); Bro-Jørgensen <sup>[249]</sup> (Au); Bu <sup>[31]</sup> (C/MoS <sub>2</sub> /BN); Cao <sup>[250]</sup> (LiTFSI/G <sub>3</sub> ); Cao <sup>[251]</sup> (Alloys); Chen <sup>[252]</sup> (Si:H); Chen <sup>[253]</sup> (Al-Cu-Li); Chen <sup>[254]</sup> (GaN); Chen <sup>[77]</sup> (CsPbI <sub>3</sub> ); Cheng <sup>[255]</sup> (AgTl <sub>2</sub> I <sub>3</sub> ); Dai <sup>[256]</sup> (C aerogels); Donadio <sup>[257]</sup> (C); Du <sup>[258]</sup> (Sn <sub>4</sub> Se <sub>10</sub> ); Feng <sup>[259]</sup> (SiO <sub>2</sub> ); Hainer <sup>[260]</sup> (MA <sub>1-x</sub> FA <sub>x</sub> PbI <sub>3</sub> ); Hao <sup>[261]</sup> (CuBiSeCl <sub>2</sub> ); Hu <sup>[262]</sup> (CL-20); Hu <sup>[263]</sup> (MoS <sub>2</sub> /WSe <sub>2</sub> ); Jia <sup>[264]</sup> (Zr); Jiang <sup>[36]</sup> (C/BN); Jiang <sup>[265]</sup> (MoS <sub>2</sub> ); Jiang <sup>[32]</sup> (MX <sub>2</sub> (M = Mo, W; X = S, Se)); Jiang <sup>[266]</sup> (MX <sub>2</sub> (M = Mo, W; X = S, Se, Te)); Kayastha <sup>[267]</sup> (BaZrS <sub>3</sub> ); Laven <sup>[268]</sup> (CsPbI <sub>3</sub> ); Li <sup>[269]</sup> (Ga <sub>2</sub> O <sub>3</sub> ); Li <sup>[270]</sup> (BeGeN <sub>2</sub> ); Li <sup>[271]</sup> (KTa <sub>1-x</sub> Nb <sub>x</sub> O <sub>3</sub> ); Li <sup>[269]</sup> (COF); Li <sup>[272]</sup> (Al, Cu, Ag); Liang <sup>[273]</sup> (C/BN); Linderalv <sup>[274]</sup> (4H-SiC); Lindgren <sup>[275]</sup> (Si, C <sub>6</sub> H <sub>6</sub> , BaTi <sub>1-x</sub> Se <sub>x</sub> O <sub>3</sub> H <sub>x</sub> ); Liu <sup>[276]</sup> (BN); Liu <sup>[277]</sup> (Ti); Liu <sup>[278]</sup> (Mg); Liu <sup>[279]</sup> (Cu <sub>7</sub> PS <sub>6</sub> ); Liu <sup>[280]</sup> (HEDs); Liu <sup>[281]</sup> (AlN-SiC); Lu <sup>[282]</sup> (C); Lu <sup>[283]</sup> (Aerogels); Luo <sup>[284]</sup> (N-Ga-Al); Lyu <sup>[285]</sup> (Pb-Se-Te-S); Moon <sup>[286]</sup> (C); Oh <sup>[287]</sup> (Si); Ouyang <sup>[288]</sup> (argyrodite); Pegolo <sup>[289]</sup> (Li <sub>3</sub> PS <sub>4</sub> ); Rosander <sup>[290]</sup> (BaZrO <sub>3</sub> ); Seifi <sup>[291]</sup> (GaAs@InAs); Sun <sup>[292]</sup> (GaN/C); Sun <sup>[293]</sup> (NbSe <sub>3</sub> ); Sun <sup>[294]</sup> (HfO <sub>2</sub> ); Tan <sup>[295]</sup>

(Continues)

TABLE 6 (Continued)

Year	Publications (major materials)
	(C/BN); Tuchinda <sup>[296]</sup> (Alloys); Wang <sup>[297]</sup> (C); Wang <sup>[298]</sup> ((AlAs) <sub>n</sub> /(InAs) <sub>n</sub> ); Wang <sup>[299]</sup> (Ne); Wang <sup>[300]</sup> (C/BN); Wang <sup>[301]</sup> (BaTiS <sub>3</sub> ); Wang <sup>[302]</sup> (GeTe/Sb <sub>2</sub> Te <sub>3</sub> ); Wang <sup>[303]</sup> ( $\beta$ -Ga <sub>2</sub> O <sub>3</sub> ); Wen <sup>[304]</sup> ((Hf, Ta, Zr, W)C); Wu <sup>[305]</sup> (MoSe <sub>2</sub> /WSe <sub>2</sub> ); Xiao <sup>[306]</sup> (C); Xiao <sup>[307]</sup> (AgSnSbTe <sub>3</sub> ); Xu <sup>[308]</sup> (LiF); Xu <sup>[309]</sup> (tobermorite); Yan <sup>[310]</sup> (Li <sub>7</sub> La <sub>3</sub> Zr <sub>2</sub> O <sub>12</sub> ); Yang <sup>[311]</sup> (Si); Yuan <sup>[312]</sup> (MgO, LiH); Yue <sup>[313]</sup> (Si/Ge); Zeng <sup>[314]</sup> (Cs <sub>3</sub> Bi <sub>2</sub> I <sub>6</sub> Cl <sub>3</sub> ); Zeraati <sup>[315]</sup> (TBCCOs); Zhang <sup>[316]</sup> (MoSi <sub>2</sub> N <sub>4</sub> ); Zhang <sup>[317]</sup> (SiC); Zhang <sup>[318]</sup> (C); Zhang <sup>[319]</sup> (Penta-PdSe <sub>2</sub> ); Zhang <sup>[320]</sup> (C/polydimethylsiloxane); Zhang <sup>[321]</sup> (Al <sub>2</sub> O <sub>3</sub> ); Zhang <sup>[322]</sup> (W-La); Zhang <sup>[323]</sup> (C); Zhou <sup>[324]</sup> (C); Zhou <sup>[325]</sup> (NbTaZr); Zhou <sup>[326]</sup> (BAs); Zhou <sup>[327]</sup> (Ga <sub>2</sub> O <sub>3</sub> /BAs); Zhou <sup>[328]</sup> (In <sub>2</sub> Se <sub>3</sub> ); Zhu <sup>[329]</sup> (HEC/Cr <sub>7</sub> C <sub>3</sub> )

Note: The table includes publications (including preprints) up to June 14, 2025.

for GPUMD, as reviewed by Dong et al.<sup>[182]</sup> up to March 2024. Nevertheless, numerous other application fields have also emerged, as summarized by Ying et al.<sup>[25]</sup> up to January 2025. Below, we briefly outline the various research fields, emphasizing key publications that pioneered the use of GPUMD in combination of NEP in these areas.

### 5.2.1 | Mechanical properties

Ying et al.<sup>[166]</sup> were the first to apply GPUMD and NEP to investigate mechanical properties in their study of a C<sub>60</sub>-based quasi-two-dimensional network. Their work demonstrated consistent results for quasi-static deformation processes when compared with quantum-mechanical calculations. Moreover, they extended the scope of their study to larger spatial and temporal scales, approaching strain rates that are almost experimentally attainable.

### 5.2.2 | Radiation damage

Liu et al.<sup>[39]</sup> expanded the NEP approach by incorporating the Ziegler-Biersack-Littmark potential,<sup>[42]</sup> applying it for the first time to investigate primary radiation damage in tungsten. They conducted large-scale MD simulations involving up to 8.1 million atoms over 240 ps using a single 40-GB A100 GPU, achieving computational efficiency comparable to that of embedded-atom-method potentials. Their study also highlighted the superior accuracy of the NEP model over embedded-atom-method potentials in capturing radiation damage in foils.

### 5.2.3 | Phase transition

The accuracy and efficiency offered by NEP models have also facilitated in-depth studies of phase transitions. Fransson et al.<sup>[142]</sup> were the first to investigate temperature-induced structural phase transitions in inorganic halide perovskites using GPUMD and NEP. Their work revealed the impact of simulation size, temperature variation rate, and the choice of exchange-correlation functionals in quantum-mechanical calculations for training data.

### 5.2.4 | Shock simulation

Shi et al.<sup>[152]</sup> initiated the study of shock compression using GPUMD and NEP. They developed a NEP model for carbon at high pressures, which demonstrated exceptional capabilities in modeling both the melting behavior and the Hugoniot line. They designed a thermodynamic pathway suitable for double shock compression experiments, facilitating the discovery of the long-sought BC8 phase of carbon.

### 5.2.5 | Short-range order

Chen et al.<sup>[177]</sup> initiated the study of short-range order in GeSn alloys using GPUMD and NEP. A compact yet representative dataset was constructed via farthest-point sampling to improve training efficiency and predictive accuracy. Through extensive statistical sampling, they uncovered intricate short-range order features that strongly impact the electronic band structure. Large-scale simulations revealed the coexistence of nanoscale short-range order domains, which is promising for optoelectronic applications.

### 5.2.6 | Ion transport

Yan et al.<sup>[233]</sup> initiated research on ion transport in solid-state electrolytes, a critical area for advancing all-solid-state battery technology. They developed a NEP model to explore the effects of lithium nonstoichiometry on ionic conductivity and phase stability in Li<sub>7</sub>La<sub>3</sub>Zr<sub>2</sub>O<sub>12</sub>. Their findings revealed that even minor deviations from stoichiometry, particularly lithium deficiency, significantly lower the activation energy for Li<sup>+</sup> diffusion in tetragonal Li<sub>7</sub>La<sub>3</sub>Zr<sub>2</sub>O<sub>12</sub>. This leads to a remarkable ten-orders-of-magnitude increase in room-temperature ionic conductivity.

### 5.2.7 | Electronic transport

Electronic and transport properties can be studied effectively using linear-scaling quantum transport approaches.<sup>[330]</sup> Fan et al.<sup>[70]</sup> combined these techniques with MD simulations,

showcasing their feasibility in modeling the electronic and thermoelectric transport properties of complex materials at finite temperatures.

### 5.2.8 | Tensorial properties

The NEP approach has also been successfully extended to modeling tensorial properties, such as electric dipole moments and polarizability, by Xu et al.<sup>[232]</sup> They demonstrated the effectiveness of this method in predicting infrared and Raman spectra for various systems, including liquid water, single molecules, and a prototypical perovskite exhibiting strong anharmonicity.

### 5.2.9 | Large NEP models

Song et al.<sup>[24]</sup> pioneered the development of large NEP models for multiple species, emphasizing the importance of focusing on elemental and binary systems during data construction. They successfully created a general-purpose NEP model for 16 metals and their arbitrary alloys, demonstrating substantially higher accuracy compared to the conventional embedded-atom method. This NEP model also achieved a computational milestone by simulating 100 million atoms using only eight 80-GB A100 GPUs.

### 5.2.10 | Hybrid Monte Carlo and molecular dynamics

Song et al.<sup>[65]</sup> were the first to apply NEP in conjunction with hybrid Monte Carlo and MD simulations. The Monte Carlo sampling with NEP is highly efficient, as it leverages the locality of the potential function. This approach holds significant promise for investigating the effects of chemical order in multicomponent systems.

### 5.2.11 | Nuclear quantum effects

Path-integral MD simulations are essential for accurately capturing nuclear quantum effects in materials. A highly efficient GPU implementation of these simulations has recently been integrated into GPUMD. Ying et al.<sup>[61]</sup> demonstrated the effectiveness of this approach by investigating thermal properties for several materials, including lithium hydride, porous metal-organic frameworks, liquid water as well as elemental aluminum.

### 5.2.12 | Melting in confined systems

Wang et al.<sup>[299]</sup> have recently used GPUMD and NEP to study the melting transition in atomistically confined layered

materials. They developed NEP models for noble gases and aluminum confined between two graphene sheets at different pressures and temperatures. Although noble gases and aluminum typically form only close-packed structures, even under the extreme conditions of white dwarf stars, they discovered tetragonal-packed configurations in the confined systems. Upon heating, they found that confined two-dimensional monolayers melt according to the two-step continuous Kosterlitz-Thouless-Halperin-Nelson-Young theory. However, multilayer solids transition continuously into an intermediate layered-hexatic phase before melting discontinuously into an isotropic liquid. This change could be qualitatively explained based on a crossover from two-dimensional topological defects to three-dimensional ones during melting as the number of layers increases.

### 5.2.13 | Hybrid NEP and anisotropic interlayer potential

Bu et al.<sup>[31]</sup> developed a hybrid computational framework that integrates a machine-learned potential, based on the NEP formalism, for intralayer interactions, with physics-based registry-dependent interlayer potential that captures anisotropic van der Waals interactions. This framework achieves near ab initio accuracy with a computational efficiency at the level of empirical potentials, enabling large-scale MD simulations of twisted van der Waals heterostructures.

### 5.2.14 | Chemical reactions

Deciphering chemical reaction mechanisms at the atomic scale is fundamental to advancing materials science, catalysis, and energy technologies. Liu et al.<sup>[278]</sup> constructed a reactive NEP model for magnesium corrosion studies by utilizing high-temperature MD to sample critical interfacial regions within substrate-interface-solution systems. This enabled the atomistic simulation of the MgOH intermediate phase formation and revealed the inward oxide/hydroxide migration mechanism governing corrosion layer growth. Hu et al.<sup>[262]</sup> also constructed a reactive NEP model to predict the reaction kinetics of 2,4,6,8,10,12-Hexanitro-2,4,6,8,10,12-hexaazaisowurtzitane (CL-20), a high energy-density material, under extreme conditions, revealing its atomic-level shock compression and thermal decomposition mechanisms. These studies demonstrate NEP's capability to resolve complex reaction pathways.

## 6 | SUMMARY AND FUTURE DIRECTIONS

In summary, we have provided a comprehensive overview of the GPUMD package, covering its development history, theoretical foundations, functionalities, and applications.

Although GPUMD is a relatively young MD package, it has been developing at a fast pace. Its robust theoretical foundation, based on an elegant formulation of many-body interatomic potentials, coupled with a well-designed GPU parallelism scheme and a versatile general-purpose machine-learned potential framework, has attracted increasing attention from researchers interested in exploring its capabilities.

Beyond its user base, the GPUMD package has also attracted numerous developers from around the globe. These contributors are working collaboratively to enhance its feature set, versatility, reliability, and efficiency, making the package increasingly robust and adaptable.

In the coming years, our efforts will focus on advancing GPUMD by further expanding its capabilities and enhancing its versatility. Building on the NEP approach, we will prioritize the incorporation of the charge degrees of freedom. This will pave the way for tackling a broader range of problems, such as those related to batteries and corrosion, further broadening the scope of applications for GPUMD. There are multiple possible strategies for combining NEP and the charge degree of freedom. The basic foundation is that the ion charges interact with each other via Coulomb forces, the evaluation of which can be either based on  $k$ -space techniques or a simple cutoff scheme. The NEP energy is then fitted to the difference between the target energy (usually based on quantum-mechanical calculations) and the Coulomb energy. The ion charge can be fitted to a particular type of target partial charge or simply be determined implicitly.<sup>[331]</sup>

Additionally, we will work on building coarse-grained models based on the NEP approach. These models will significantly extend both the spatial and temporal scales achievable in MD simulations with GPUMD, opening up new possibilities for studying large systems and long-time phenomena. One straightforward strategy is force-matching, where the forces acting between the coarse-grained sites are systematically derived from the net forces experienced by those sites in all-atom simulations based on an all-atom NEP model. The coarse-grained system can also be described by a coarse-grained NEP model that is mathematically similar to the all-atom NEP model. Moreover, the separable natural evolution strategy in NEP is a powerful derivative-free black-box optimizer, which can conveniently take into consideration of experimental data as well as complex physical quantities during the training to enhance the reliability of the coarse-grained NEP models.

To push the boundaries of efficiency and accuracy, we plan to develop Monte Carlo sampling methods, enhanced sampling methods, and other time-acceleration techniques. These advancements will enable GPUMD to overcome the limitations of conventional MD simulations, allowing for a more comprehensive exploration of complex systems.

A direction that is seemingly unrelated to MD simulations is the development of general-purpose tight-binding models for electrons. These models will be an extension of the NEP framework, bridging the strengths of quantum transport methodologies<sup>[330]</sup> and MD to enable more

accurate and efficient simulations of electronic properties in spatially complex materials.

## AUTHOR CONTRIBUTIONS

**Ke Xu:** Conceptualization; methodology; software; data curation; writing—review and editing; writing—original draft; visualization; investigation; validation; formal analysis. **Hekai Bu:** Methodology; software; data curation; investigation; validation; formal analysis; writing—review and editing. **Shuning Pan:** Methodology; software; data curation; investigation; validation; formal analysis; writing—review and editing. **Eric Lindgren:** Methodology; software; data curation; investigation; validation; formal analysis; writing—review and editing. **Yongchao Wu:** Methodology; software; data curation; investigation; validation; formal analysis; writing—review and editing. **Yong Wang:** Methodology; software; data curation; investigation; validation; formal analysis; writing—review and editing. **Jiahui Liu:** Methodology; software; data curation; investigation; validation; formal analysis; writing—review and editing. **Keke Song:** Methodology; software; data curation; investigation; validation; formal analysis; writing—review and editing. **Bin Xu:** Methodology; software; data curation; investigation; validation; formal analysis; writing—review and editing. **Yifan Li:** Methodology; software; data curation; investigation; validation; formal analysis; writing—review and editing. **Tobias Hainer:** Methodology; software; data curation; investigation; validation; formal analysis; writing—review and editing. **Lucas Svensson:** Methodology; software; data curation; investigation; validation; formal analysis; writing—review and editing. **Julia Wiktor:** Methodology; software; data curation; investigation; validation; formal analysis; writing—review and editing. **Rui Zhao:** Methodology; software; data curation; investigation; validation; formal analysis; writing—review and editing. **Hongfu Huang:** Methodology; software; data curation; investigation; validation; formal analysis; writing—review and editing. **Cheng Qian:** Methodology; software; data curation; investigation; validation; formal analysis; writing—review and editing. **Shuo Zhang:** Methodology; software; data curation; investigation; validation; formal analysis; writing—review and editing. **Zezhu Zeng:** Methodology; software; data curation; investigation; validation; formal analysis; writing—review and editing. **Bohan Zhang:** Methodology; software; data curation; investigation; validation; formal analysis; writing—review and editing. **Benrui Tang:** Methodology; software; data curation; investigation; validation; formal analysis; writing—review and editing. **Yang Xiao:** Methodology; software; data curation; investigation; validation; formal analysis; writing—review and editing. **Zihan Yan:** Methodology; software; data curation; investigation; validation; formal analysis; writing—review and editing. **Jiuyang Shi:** Methodology; software; data curation; investigation; validation; formal analysis; writing—review and editing. **Zhixin Liang:** Methodology; software; data curation; investigation; validation; formal analysis; writing—review and editing. **Junjie**

**Wang:** Methodology; software; data curation; investigation; validation; formal analysis; writing—review and editing. **Ting Liang:** Methodology; software; data curation; investigation; validation; formal analysis; writing—review and editing. **Shuo Cao:** Methodology; software; data curation; investigation; validation; formal analysis; writing—review and editing. **Yanzhou Wang:** Methodology; software; data curation; investigation; validation; formal analysis; writing—review and editing. **Penghua Ying:** Methodology; software; data curation; investigation; validation; formal analysis; writing—review and editing. **Nan Xu:** Methodology; software; data curation; investigation; validation; formal analysis; writing—review and editing. **Chengbing Chen:** Methodology; software; data curation; investigation; validation; formal analysis; writing—review and editing. **Yuwen Zhang:** Methodology; software; data curation; investigation; validation; formal analysis; writing—review and editing. **Zherui Chen:** Methodology; software; data curation; investigation; validation; formal analysis; writing—review and editing. **Xin Wu:** Methodology; software; data curation; investigation; validation; formal analysis; writing—review and editing. **Wenwu Jiang:** Methodology; software; data curation; investigation; validation; formal analysis; writing—review and editing. **Esme Berger:** Methodology; software; data curation; investigation; validation; formal analysis; writing—review and editing. **Yanlong Li:** Methodology; software; data curation; investigation; validation; formal analysis; writing—review and editing. **Shunda Chen:** Methodology; software; data curation; investigation; validation; formal analysis; writing—review and editing. **Alexander J. Gabourie:** Methodology; software; data curation; investigation; validation; formal analysis; writing—review and editing. **Haikuan Dong:** Methodology; software; data curation; investigation; validation; formal analysis; writing—review and editing. **Shiyun Xiong:** Methodology; software; data curation; investigation; validation; formal analysis; writing—review and editing. **Ning Wei:** Supervision; resources; funding acquisition; writing—review and editing; project administration. **Yue Chen:** Writing—review and editing; resources; project administration; funding acquisition; supervision. **Jianbin Xu:** Supervision; funding acquisition; project administration; resources; writing—review and editing. **Feng Ding:** Supervision; funding acquisition; project administration; resources; writing—review and editing. **Zhimei Sun:** Supervision; funding acquisition; project administration; resources; writing—review and editing. **Tapio Ala-Nissila:** Supervision; resources; project administration; funding acquisition; writing—review and editing. **Ari Harju:** Supervision; project administration; resources; funding acquisition; writing—review and editing. **Jincheng Zheng:** Supervision; funding acquisition; project administration; resources; writing—review and editing. **Pengfei Guan:** Supervision; funding acquisition; project administration; resources; writing—review and editing. **Paul Erhart:** Supervision; funding acquisition; resources; writing—review and editing; project administration. **Jian Sun:**

Supervision; funding acquisition; project administration; resources; writing—review and editing. **Wengen Ouyang:** Supervision; funding acquisition; project administration; resources; writing—review and editing. **Yanjing Su:** Supervision; funding acquisition; project administration; resources; writing—review and editing. **Zheyong Fan:** Writing—review and editing; resources; supervision; funding acquisition; project administration; writing—original draft; conceptualization; methodology; software; formal analysis; validation; investigation; visualization; data curation.

## AFFILIATIONS

- <sup>1</sup>College of Physical Science and Technology, Bohai University, Jinzhou, China
- <sup>2</sup>Department of Engineering Mechanics, School of Civil Engineering, Wuhan University, Wuhan, China
- <sup>3</sup>National Laboratory of Solid State Microstructures, School of Physics and Collaborative Innovation Center of Advanced Microstructures, Nanjing University, Nanjing, China
- <sup>4</sup>Department of Physics, Chalmers University of Technology, Gothenburg, Sweden
- <sup>5</sup>State Key Laboratory of Explosion Science and Safety Protection, Beijing Institute of Technology, Beijing, China
- <sup>6</sup>Department of Chemistry, Princeton University, Princeton, New Jersey, USA
- <sup>7</sup>Beijing Advanced Innovation Center for Materials Genome Engineering, University of Science and Technology Beijing, Beijing, China
- <sup>8</sup>Advanced Interdisciplinary Science Research (AiR) Center, Ningbo Institute of Materials Technology and Engineering, Chinese Academy of Sciences, Ningbo, China
- <sup>9</sup>School of Mechanical and Electrical Engineering, Xinyu University, Xinyu, China
- <sup>10</sup>School of Materials Science and Engineering, Beihang University, Beijing, China
- <sup>11</sup>Suzhou Laboratory, Suzhou, China
- <sup>12</sup>School of Mechanical Engineering, Jiangnan University, Wuxi, China
- <sup>13</sup>Department of Mechanical Engineering, The University of Hong Kong, Hong Kong, China
- <sup>14</sup>School of Engineering, Westlake University, Hangzhou, China
- <sup>15</sup>Department of Electronic Engineering and Materials Science and Technology Research Center, The Chinese University of Hong Kong, Hong Kong, China
- <sup>16</sup>Department of Applied Physics, MSP Group, QTF Centre of Excellence, Aalto University, Espoo, Finland
- <sup>17</sup>Department of Physical Chemistry, School of Chemistry, Tel Aviv University, Tel Aviv, Israel
- <sup>18</sup>College of Chemical and Biological Engineering, Zhejiang University, Hangzhou, China
- <sup>19</sup>College of Physics and Electronic Information Engineering, Guilin University of Technology, Guilin, China
- <sup>20</sup>Eastern Institute for Advanced Study, Eastern Institute of Technology, Ningbo, China
- <sup>21</sup>Future Technology School, Shenzhen Technology University, Shenzhen, China
- <sup>22</sup>College of Applied Sciences, Shenzhen University, Shenzhen, China
- <sup>23</sup>Institute of Industrial Science, The University of Tokyo, Tokyo, Japan
- <sup>24</sup>Key Laboratory of Computing Power Network and Information Security, Ministry of Education, Shandong Computer Science Center (National Supercomputer Center in Jinan), Qilu University of Technology (Shandong Academy of Sciences), Jinan, China
- <sup>25</sup>Department of Civil and Environmental Engineering, George Washington University, Washington, DC, USA
- <sup>26</sup>DeepSim, Inc., Mountain View, California, USA
- <sup>27</sup>Guangzhou Key Laboratory of Low-Dimensional Materials and Energy Storage Devices, School of Materials and Energy, Guangdong University of Technology, Guangzhou, China
- <sup>28</sup>Department of Mathematical Sciences, Interdisciplinary Centre for Mathematical Modelling, Loughborough University, Loughborough, UK
- <sup>29</sup>Varian Medical Systems, a Siemens Healthineers Company, Helsinki, Finland

<sup>30</sup>Department of New Energy Science and Engineering, Xiamen University Malaysia, Sepang, Malaysia

<sup>31</sup>Department of Physics, Xiamen University Malaysia, Sepang, Malaysia

<sup>32</sup>Department of Physics, Xiamen University, Xiamen, China

<sup>33</sup>Wallenberg Initiative Materials Science for Sustainability, Chalmers University of Technology, Gothenburg, Sweden

<sup>34</sup>State Key Laboratory of Water Resources Engineering and Management, Wuhan University, Wuhan, China

## ACKNOWLEDGMENTS

This work was supported by the National Science and Technology Advanced Materials Major Program of China (No. 2024ZD0606900). W. Ouyang acknowledges the financial support from the National Natural Science Foundation of China (No. 12472099) and the Fundamental Research Funds for the Central Universities (No. 2042025kf0050). S. Pan, Y. Wang, J. Shi, Z. Liang, J. Wang, and J. Sun acknowledge the financial support from the National Natural Science Foundation of China (Nos. 12125404, T2495231, and 123B2049), the Basic Research Program of Jiangsu (Nos. BK20233001 and BK20241253), the Jiangsu Funding Program for Excellent Postdoctoral Talent (Nos. 2024ZB002 and 2024ZB075), the Postdoctoral Fellowship Program of CPSF (No. GZC20240695), the AI & AI for the Science Program of Nanjing University, and the Fundamental Research Funds for the Central Universities, as well as the computational resources provided by the High Performance Computing Center of Collaborative Innovation Center of Advanced Microstructures and the high-performance supercomputing center of Nanjing University. P. Guan acknowledges the financial support by the National Natural Science Foundation of China (No. T2325004). E. Lindgren, T. Hainer, L. Svensson, J. Wiktor, E. Berger, and P. Erhart gratefully acknowledge funding from the Swedish Foundation for Strategic Research (GSn15-0008 and FFL21-0129), the Swedish Research Council (Nos. 2020-04935 and 2021-05072), the Knut and Alice Wallenberg Foundation (Nos. 2023.0032 and 2024.0042), and the European Research Council (ERC Starting Grant No. 101162195) as well as computational resources provided by the National Academic Infrastructure for Supercomputing in Sweden at NSC, PDC, and C3SE partially funded by the Swedish Research Council through grant agreement no. 2022-06725, as well as the Berzelius resource provided by the Knut and Alice Wallenberg Foundation at NSC. T.A.-N. and Y.W. have been supported in part by the Academy of Finland through its QTF Center of Excellence program (project no. 312298) and European Union—NextGenerationEU instrument grant 353298. Computational resources by the CSC IT Center for Finland and the Aalto Science-IT are also gratefully acknowledged.

## CONFLICT OF INTEREST STATEMENT

The authors declare no conflicts of interest.

## DATA AVAILABILITY STATEMENT

The source code for GPUMD (version 4.0) is available at the Zenodo repository <https://doi.org/10.5281/zenodo.15299>

684<sup>[26]</sup> and the GitHub repository <https://github.com/brucefan1983/GPUMD/releases/tag/v4.0>.

## ORCID

Hongfu Huang  <https://orcid.org/0000-0002-6126-5622>

Zihan Yan  <https://orcid.org/0000-0002-8911-6549>

Zhimei Sun  <https://orcid.org/0000-0002-4438-5032>

Zheyong Fan  <https://orcid.org/0000-0002-2253-8210>

## REFERENCES

1. Abraham MJ, Murtola T, Schulz R, et al. GROMACS: high performance molecular simulations through multi-level parallelism from laptops to supercomputers. *SoftwareX*. 2015;1-2:19-25.
2. Thompson AP, Aktulga HM, Berger R, et al. LAMMPS – a flexible simulation tool for particle-based materials modeling at the atomic, meso, and continuum scales. *Comput Phys Commun*. 2022;271:108171.
3. Eastman P, Galvelis R, Peláez RP, et al. OpenMM 8: molecular dynamics simulation with machine learning potentials. *J Phys Chem B*. 2024;128(1):109-116.
4. Talirz L, Ghiringhelli LM, Smit B. Trends in atomistic simulation software usage [Article v1.0]. *Living J Comput Mol Sci*. 2021;3(1):1483.
5. Talirz L. Ltalirz/Atomistic-Software: v2025.4.20; 2025.
6. Fan Z, Chen W, Vierimaa V, Harju A. Efficient molecular dynamics simulations with many-body potentials on graphics processing units. *Comput Phys Commun*. 2017;218:10-16.
7. Fan Z, Wang Y, Ying P, et al. GPUMD: a package for constructing accurate machine-learned potentials and performing highly efficient atomistic simulations. *J Chem Phys*. 2022;157(11):114801.
8. Anderson JA, Glaser J, Glotzer SC. HOOMD-blue: a Python package for high-performance molecular dynamics and hard particle Monte Carlo simulations. *Comput Mater Sci*. 2020;173:109363.
9. Zhu Y-L, Liu H, Li Z-W, Qian H-J, Milano G, Lu Z-Y. GALA-MOST: GPU-accelerated large-scale molecular simulation toolkit. *J Comput Chem*. 2013;34(25):2197-2211.
10. Xu J-L, Guo S-H, Zhen M, Yu Z-C, Zhu Y-L, Lu Z-Y. PyGAMD: Python GPU-accelerated molecular dynamics software. *MGE Adv*. 2025:1.
11. Fan Z, Siro T, Harju A. Accelerated molecular dynamics force evaluation on graphics processing units for thermal conductivity calculations. *Comput Phys Commun*. 2013;184(5):1414-1425.
12. Fan Z, Pereira LFC, Wang H-Q, Zheng J-C, Donadio D, Harju A. Force and heat current formulas for many-body potentials in molecular dynamics simulations with applications to thermal conductivity calculations. *Phys Rev B*. 2015;92(9):094301.
13. Daw MS, Baskes MI. Embedded-atom method: derivation and application to impurities, surfaces, and other defects in metals. *Phys Rev B*. 1984;29(12):6443-6453.
14. Finnis MW, Sinclair JE. A simple empirical N-body potential for transition metals. *Philos Mag A*. 1984;50(1):45-55.
15. Stillinger FH, Weber TA. Computer simulation of local order in condensed phases of silicon. *Phys Rev B*. 1985;31(8):5262-5271.
16. Tersoff J. Empirical interatomic potential for carbon, with applications to amorphous carbon. *Phys Rev Lett*. 1988;61(25):2879-2882.
17. Fan Z, Dong H, Harju A, Ala-Nissila T. Homogeneous nonequilibrium molecular dynamics method for heat transport and spectral decomposition with many-body potentials. *Phys Rev B*. 2019;99(6):064308.
18. Fan Z, Pereira LFC, Hirvonen P, et al. Thermal conductivity decomposition in two-dimensional materials: application to graphene. *Phys Rev B*. 2017;95(14):144309.
19. Gabourie AJ, Fan Z, Ala-Nissila T, Pop E. Spectral decomposition of thermal conductivity: comparing velocity decomposition methods in homogeneous molecular dynamics simulations. *Phys Rev B*. 2021;103(20):205421.

20. Fan Z, Wang Y, Gu X, Qian P, Su Y, Ala-Nissila T. A minimal Tersoff potential for diamond silicon with improved descriptions of elastic and phonon transport properties. *J Phys Condens Matter*. 2019;32(13):135901.
21. Brorsson J, Hashemi A, Fan Z, et al. Efficient calculation of the lattice thermal conductivity by atomistic simulations with ab initio accuracy. *Adv Theor Simulat*. 2022;5(2):2100217.
22. Fan Z, Zeng Z, Zhang C, et al. Neuroevolution machine learning potentials: combining high accuracy and low cost in atomistic simulations and application to heat transport. *Phys Rev B*. 2021;104(10):104309.
23. Fan Z. Improving the accuracy of the neuroevolution machine learning potential for multi-component systems. *J Phys Condens Matter*. 2022;34(12):125902.
24. Song K, Zhao R, Liu J, et al. General-purpose machine-learned potential for 16 elemental metals and their alloys. *Nat Commun*. 2024;15(1):10208.
25. Ying P, Qian C, Zhao R, et al. Advances in modeling complex materials: the rise of neuroevolution potentials. *Chem Phys Rev*. 2025;6(1):011310.
26. Fan Z, Ke X, Bu H, et al. Brucefan1983/gpumd: Gpumd-v4.0. Zenodo. 2025.
27. Fan Z. *CUDA Programming*. Tsinghua University Press; 2020.
28. Fan Z. *Molecular Dynamics Simulation*. Chemical Industry Press; 2024.
29. Lennard-Jones JE. Cohesion. *Proc Phys Soc*. 1931;43(5):461-482.
30. Zeng J, Zhang D, Lu D, et al. DeePMD-kit v2: a software package for deep potential models. *J Chem Phys*. 2023;159(5):054801.
31. Bu H, Jiang W, Ying P, Fan Z, Ouyang W. Accurate modeling of LEGO-like vdW heterostructures: integrating machine learned with anisotropic interlayer potentials. *arXiv:2504.12985 [physics.comp-ph]*. 2025.
32. Jiang W, Liang T, Bu H, Xu J, Ouyang W. Moiré-driven interfacial thermal transport in twisted transition metal dichalcogenides. *ACS Nano*. 2025;19(17):16287-16296.
33. Ouyang W, Mandelli D, Urbakh M, Hod O. Nanoserpents: graphene nanoribbon motion on two-dimensional hexagonal materials. *Nano Lett*. 2018;18(9):6009-6016.
34. Ouyang W, Azuri I, Mandelli D, et al. Mechanical and tribological properties of layered materials under high pressure: assessing the importance of many-body dispersion effects. *J Chem Theor Comput*. 2020;16(1):666-676.
35. Jiang W, Sofer R, Gao X, et al. Anisotropic interlayer force field for group-VI transition metal dichalcogenides. *J Phys Chem A*. 2023;127(46):9820-9830.
36. Jiang W, Sofer R, Gao X, et al. Anisotropic interlayer force field for interfaces of graphene and h-BN with transition metal dichalcogenides. *J Phys Chem C*. 2025;129(2):1417-1427.
37. Eriksson F, Fransson E, Erhart P. The hiphive package for the extraction of high-order force constants by machine learning. *Adv Theor Simulat*. 2019;2(5):1800184.
38. Behler J, Parrinello M. Generalized neural-network representation of high-dimensional potential-energy surfaces. *Phys Rev Lett*. 2007;98(14):146401.
39. Liu J, Byggmästar J, Fan Z, Qian P, Su Y. Large-scale machine-learning molecular dynamics simulation of primary radiation damage in tungsten. *Phys Rev B*. 2023;108(5):054312.
40. Ying P, Fan Z. Combining the D3 dispersion correction with the neuroevolution machine-learned potential. *J Phys Condens Matter*. 2023;36(12):125901.
41. Grimme S, Ehrlich S, Goerigk L. Effect of the damping function in dispersion corrected density functional theory. *J Comput Chem*. 2011;32(7):1456-1465.
42. Ziegler JF, Biersack JP. The stopping and range of ions in matter. In: Bromley DA, ed. *Treatise on Heavy-Ion Science: Volume 6: Astrophysics, Chemistry, and Condensed Matter*. Springer US; 1985:93-129.
43. Liang T, Xu K, Lindgren E, et al. NEP89: universal neuroevolution potential for inorganic and organic materials across 89 elements. *arXiv:2504.21286 [cond-mat.mtrl-sci]*. 2025.
44. Batzner S, Musaelian A, Sun L, et al. E(3)-equivariant graph neural networks for data-efficient and accurate interatomic potentials. *Nat Commun*. 2022;13(1):2453.
45. Batatia I, Kovacs DP, Simm G, Ortner C, Csányi G. MACE: higher order equivariant message passing neural networks for fast and accurate force fields. *Adv Neural Inf Process Syst*. 2022;35:11423.
46. Swope WC, Andersen HC, Berens PH, Wilson KR. A computer simulation method for the calculation of equilibrium constants for the formation of physical clusters of molecules: application to small water clusters. *J Chem Phys*. 1982;76(1):637-649.
47. Tuckerman ME. *Statistical Mechanics: Theory and Molecular Simulation*. Oxford University Press; 2023.
48. Berendsen HJC, Postma JPM, van Gunsteren WF, DiNola A, Haak JR. Molecular dynamics with coupling to an external bath. *J Chem Phys*. 1984;81(8):3684-3690.
49. Bussi G, Donadio D, Parrinello M. Canonical sampling through velocity rescaling. *J Chem Phys*. 2007;126(1):014101.
50. Bussi G, Parrinello M. Accurate sampling using Langevin dynamics. *Phys Rev E*. 2007;75(5):056707.
51. Leimkuhler B, Matthews C. Rational construction of stochastic numerical methods for molecular sampling. *Appl Math Res eXpress*. 2013;2013:34.
52. Bernetti M, Bussi G. Pressure control using stochastic cell rescaling. *J Chem Phys*. 2020;153(11):114107.
53. Li Z, Xiong S, Sievers C, et al. Influence of thermostating on nonequilibrium molecular dynamics simulations of heat conduction in solids. *J Chem Phys*. 2019;151(23):234105.
54. Frenkel D, Ladd AJC. New Monte Carlo method to compute the free energy of arbitrary solids. Application to the fcc and hcp phases of hard spheres. *J Chem Phys*. 1984;81(7):3188-3193.
55. Freitas R, Asta M, de Koning M. Nonequilibrium free-energy calculation of solids using LAMMPS. *Comput Mater Sci*. 2016;112:333-341.
56. Cahahuaringa S, Antonelli A. Non-equilibrium free-energy calculation of phase-boundaries using LAMMPS. *Comput Mater Sci*. 2022;207:111275.
57. Paula Leite R, Freitas R, Azevedo R, de Koning M. The Uhlenbeck-Ford model: exact virial coefficients and application as a reference system in fluid-phase free-energy calculations. *J Chem Phys*. 2016;145(19):194101.
58. Pan S, Shi J, Liang Z, et al. Shock compression pathways to pyrite silica from machine learning simulations. *Phys Rev B*. 2024;110(22):224101.
59. Ravelo R, Holian BL, Germann TC, Lomdahl PS. Constant-stress Hugoniot method for following the dynamical evolution of shocked matter. *Phys Rev B*. 2004;70(1):014103.
60. Ceriotti M, Parrinello M, Markland TE, Manolopoulos DE. Efficient stochastic thermostating of path integral molecular dynamics. *J Chem Phys*. 2010;133(12):124104.
61. Ying P, Zhou W, Svensson L, et al. Highly efficient path-integral molecular dynamics simulations with GPUMD using neuroevolution potentials: case studies on thermal properties of materials. *J Chem Phys*. 2025;162(6):064109.
62. Craig IR, Manolopoulos DE. Quantum statistics and classical mechanics: real time correlation functions from ring polymer molecular dynamics. *J Chem Phys*. 2004;121(8):3368-3373.
63. Rossi M, Ceriotti M, Manolopoulos DE. How to remove the spurious resonances from ring polymer molecular dynamics. *J Chem Phys*. 2014;140(23):234116.
64. Korol R, Bou-Rabee N, Miller I, Thomas F. Cayley modification for strongly stable path-integral and ring-polymer molecular dynamics. *J Chem Phys*. 2019;151(12):124103.
65. Song K, Liu J, Chen S, Fan Z, Su Y, Qian P. Solute segregation in polycrystalline aluminum from hybrid Monte Carlo and molecular

- dynamics simulations with a unified neuroevolution potential. *arXiv:2404.13694 [cond-mat.mtrl-sci]*. 2024.
66. Sadigh B, Erhart P, Stukowski A, Caro A, Martinez E, Zepeda-Ruiz L. Scalable parallel Monte Carlo algorithm for atomistic simulations of precipitation in alloys. *Phys Rev B*. 2012;85(18):184203.
  67. Sadigh B, Erhart P. Calculation of excess free energies of precipitates via direct thermodynamic integration across phase boundaries. *Phys Rev B*. 2012;86(13):134204.
  68. Rahm JM, Lofgren J, Fransson E, Erhart P. A tale of two phase diagrams: interplay of ordering and hydrogen uptake in Pd-Au-H. *Acta Mater*. 2021;211:116893.
  69. Stukowski A. Visualization and analysis of atomistic simulation data with OVITO – the open visualization tool. *Model Simulat Mater Sci Eng*. 2010;18(1):015012.
  70. Fan Z, Xiao Y, Wang Y, Ying P, Chen S, Dong H. Combining linear-scaling quantum transport and machine-learning molecular dynamics to study thermal and electronic transports in complex materials. *J Phys Condens Matter*. 2024;36(24):245901.
  71. Lindgren E, Rahm M, Fransson E, et al. calorine: a Python package for constructing and sampling neuroevolution potential models. *J Open Source Softw*. 2024;9(95):6264.
  72. Fransson E, Slabanja M, Erhart P, Wahnström G. DYNASOR – a tool for extracting dynamical structure factors and current correlation functions from molecular dynamics simulations. *Adv Theor Simulat*. 2021;4(2):2000240.
  73. Berger E, Fransson E, Eriksson F, et al. Dynasor 2: from simulation to experiment through correlation functions. *Comput Phys Commun*. 2025;109759.
  74. Wang J, Gao H, Han Y, et al. MAGUS: machine learning and graph theory assisted universal structure searcher. *Natl Sci Rev*. 2023;10(7):nwad128.
  75. Han Y, Ding C, Wang J, et al. Efficient crystal structure prediction based on the symmetry principle. *Nat Comput Sci*. 2025;5(3):255-267.
  76. Wu Y-C, Shao J-L. mdapy: a flexible and efficient analysis software for molecular dynamics simulations. *Comput Phys Commun*. 2023;290:108764.
  77. Chen C, Li Y, Zhao R, et al. NepTrain and NEPTrainKit: automated active learning and visualization toolkit for neuroevolution potentials. *arXiv:2506.01868 [cs.LG]*. 2025.
  78. Liang T, Jiang W, Xu K, et al. PYSED: a tool for extracting kinetic-energy-weighted phonon dispersion and lifetime from molecular dynamics simulations. *arXiv:2505.00353 [physics.comp-ph]*. 2025.
  79. Larsen AH, Mortensen JJ, Blomqvist J, et al. The atomic simulation environment – a Python library for working with atoms. *J Phys Condens Matter*. 2017;29(27):273002.
  80. Hirvonen P, Ervasti MM, Fan Z, et al. Multiscale modeling of polycrystalline graphene: a comparison of structure and defect energies of realistic samples from phase field crystal models. *Phys Rev B*. 2016;94(3):035414.
  81. Mortazavi B, Fan Z, Pereira LFC, Harju A, Rabczuk T. Amorphized graphene: a stiff material with low thermal conductivity. *Carbon*. 2016;103:318-326.
  82. Azizi K, Hirvonen P, Fan Z, et al. Kapitza thermal resistance across individual grain boundaries in graphene. *Carbon*. 2017;125:384-390.
  83. Fan Z, Hirvonen P, Pereira LFC, et al. Bimodal grain-size scaling of thermal transport in polycrystalline graphene from large-scale molecular dynamics simulations. *Nano Lett*. 2017;17(10):5919-5924.
  84. Fan Z, Uppstu A, Harju A. Dominant source of disorder in graphene: charged impurities or ripples? *2D Mater*. 2017;4(2):025004.
  85. Hirvonen P, Fan Z, Ervasti MM, Harju A, Elder KR, Ala-Nissila T. Energetics and structure of grain boundary triple junctions in graphene. *Sci Rep*. 2017;7(1):4754.
  86. Mortazavi B, Lherbier A, Fan Z, Harju A, Rabczuk T, Charlier J-C. Thermal and electronic transport characteristics of highly stretchable graphene kirigami. *Nanoscale*. 2017;9(42):16329-16341.
  87. Dong H, Fan Z, Shi L, Harju A, Ala-Nissila T. Equivalence of the equilibrium and the nonequilibrium molecular dynamics methods for thermal conductivity calculations: from bulk to nanowire silicon. *Phys Rev B*. 2018;97(9):094305.
  88. Dong H, Hirvonen P, Fan Z, Ala-Nissila T. Heat transport in pristine and polycrystalline single-layer hexagonal boron nitride. *Phys Chem Chem Phys*. 2018;20(38):24602-24612.
  89. Fan Z, Vierimaa V, Harju A. GPUQT: an efficient linear-scaling quantum transport code fully implemented on graphics processing units. *Comput Phys Commun*. 2018;230:113-120.
  90. Hirvonen P, La Boissonière GM, Fan Z, et al. Grain extraction and microstructural analysis method for two-dimensional poly and quasicrystalline solids. *Phys Rev Mater*. 2018;2:103603.
  91. Mortazavi B, Makaremi M, Shahrokhi M, Fan Z, Rabczuk T. N-graphdiyne two-dimensional nanomaterials: semiconductors with low thermal conductivity and high stretchability. *Carbon*. 2018;137:57-67.
  92. Rajabpour A, Fan Z, Vaez Allaei SM. Inter-layer and intra-layer heat transfer in bilayer/monolayer graphene van der Waals heterostructure: Is there a Kapitza resistance analogous? *Appl Phys Lett*. 2018;112(23):233104.
  93. Xu K, Fan Z, Zhang J, Wei N, Ala-Nissila T. Thermal transport properties of single-layer black phosphorus from extensive molecular dynamics simulations. *Model Simulat Mater Sci Eng*. 2018;26(8):085001.
  94. Gu X, Fan Z, Bao H, Zhao CY. Revisiting phonon-phonon scattering in single-layer graphene. *Phys Rev B*. 2019;100(6):064306.
  95. Isaeva L, Barbalinardo G, Donadio D, Baroni S. Modeling heat transport in crystals and glasses from a unified lattice-dynamical approach. *Nat Commun*. 2019;10(1):3853.
  96. Xu K, Gabourie AJ, Hashemi A, et al. Thermal transport in MoS<sub>2</sub> from molecular dynamics using different empirical potentials. *Phys Rev B*. 2019;99(5):054303.
  97. Bea EA, Carusela MF, Soba A, Monastra AG, Viotti AMM. Thermal conductance of structured silicon nanocrystals. *Model Simulat Mater Sci Eng*. 2020;28(7):075004.
  98. Dong H, Fan Z, Qian P, Ala-Nissila T, Su Y. Thermal conductivity reduction in carbon nanotube by fullerene encapsulation: a molecular dynamics study. *Carbon*. 2020;161:800-808.
  99. Fu B, Parrish KD, Kim H-Y, Tang G, McGaughey AJH. Phonon confinement and transport in ultrathin films. *Phys Rev B*. 2020;101(4):045417.
  100. Gabourie AJ, Suryavanshi SV, Farimani AB, Pop E. Reduced thermal conductivity of supported and encased monolayer and bilayer MoS<sub>2</sub>. *2D Mater*. 2020;8(1):011001.
  101. Wu X, Han Q. Thermal conductivity of defective graphene: an efficient molecular dynamics study based on graphics processing units. *Nanotechnology*. 2020;31(21):215708.
  102. Wu X, Han Q. Thermal conductivity of monolayer hexagonal boron nitride: from defective to amorphous. *Comput Mater Sci*. 2020;184:109938.
  103. Barbalinardo G, Chen Z, Dong H, Fan Z, Donadio D. Ultrahigh convergent thermal conductivity of carbon nanotubes from comprehensive atomistic modeling. *Phys Rev Lett*. 2021;127(2):025902.
  104. Chen X-K, Hu X-Y, Jia P, Xie Z-X, Liu J. Tunable anisotropic thermal transport in porous carbon foams: the role of phonon coupling. *Int J Mech Sci*. 2021;206:106576.
  105. Dong H, Hirvonen P, Fan Z, Qian P, Su Y, Ala-Nissila T. Heat transport across graphene/hexagonal-BN tilted grain boundaries from phase-field crystal model and molecular dynamics simulations. *J Appl Phys*. 2021;130(23):235102.
  106. Dong H, Xiong S, Fan Z, Qian P, Su Y, Ala-Nissila T. Interpretation of apparent thermal conductivity in finite systems from equilibrium molecular dynamics simulations. *Phys Rev B*. 2021;103(3):035417.
  107. Du Y, Ying P, Zhang J. Prediction and optimization of the thermal transport in hybrid carbon-boron nitride honeycombs using machine learning. *Carbon*. 2021;184:492-503.
  108. Kim SE, Mujid F, Rai A, et al. Extremely anisotropic van der Waals thermal conductors. *Nature*. 2021;597(7878):660-665.

109. Lundgren NW, Barbalinardo G, Donadio D. Mode localization and suppressed heat transport in amorphous alloys. *Phys Rev B*. 2021;103(2):024204.
110. So S, Kim J-Y, Kim D, Lee J-H. Recovery of thermal transport in atomic-layer-deposition-healed defective graphene. *Carbon*. 2021;180:77-84.
111. Wang H, Cheng Y, Fan Z, et al. Anomalous thermal conductivity enhancement in low dimensional resonant nanostructures due to imperfections. *Nanoscale*. 2021;13(22):10010-10015.
112. Wu X, Han Q. Phonon thermal transport across multilayer graphene/hexagonal boron nitride van der Waals heterostructures. *ACS Appl Mater Interfaces*. 2021;13(27):32564-32578.
113. Wu X, Han Q. Semidefective graphene/h-BN in-plane heterostructures: enhancing interface thermal conductance by topological defects. *J Phys Chem C*. 2021;125(4):2748-2760.
114. Zhang Z, Guo Y, Bescond M, Chen J, Nomura M, Volz S. Generalized decay law for particlelike and wavelike thermal phonons. *Phys Rev B*. 2021;103(18):184307.
115. Cheng Y, Xiong S, Zhang T. Enhancing the coherent phonon transport in SiGe nanowires with dense Si/Ge interfaces. *Nanomaterials*. 2022;12(24):4373.
116. Dong H, Fan Z, Qian P, Su Y. Exactly equivalent thermal conductivity in finite systems from equilibrium and nonequilibrium molecular dynamics simulations. *Phys E Low-Dimens Syst Nanostruct*. 2022;144:115410.
117. Feng H, Zhang K, Wang X, Zhang G, Guo X. Thermal transport of bilayer graphene: a homogeneous nonequilibrium molecular dynamics study. *Phys Scri*. 2022;97(4):045704.
118. Gabourie AJ, Köroğlu Ç, Pop E. Substrate-dependence of monolayer MoS<sub>2</sub> thermal conductivity and thermal boundary conductance. *J Appl Phys*. 2022;131(19):195103.
119. Jin S, Zhang Z, Guo Y, Chen J, Nomura M, Volz S. Optimization of interfacial thermal transport in Si/Ge heterostructure driven by machine learning. *Int J Heat Mass Tran*. 2022;182:122014.
120. Li Z-H, Lu C, Shi A, Zhao S, Ou B, Wei N. A multi-scale study on deformation and failure process of metallic structures in extreme environment. *Int J Mol Sci*. 2022;23(22):14437.
121. Li K, Cheng Y, Dou M, Zeng W, Volz S, Xiong S. Tuning the anisotropic thermal transport in 110-silicon membranes with surface resonances. *Nanomaterials*. 2022;12(1):123.
122. Li K, Cheng Y, Wang H, et al. Phonon resonant effect in silicon membranes with different crystallographic orientations. *Int J Heat Mass Tran*. 2022;183:122144.
123. Liang T, Xu K, Han M, et al. Abnormally high thermal conductivity in fivefold twinned diamond nanowires. *Mater Today Phys*. 2022;25:100705.
124. Sha W, Dai X, Chen S, Guo F. Phonon thermal transport in graphene/h-BN superlattice monolayers. *Diam Relat Mater*. 2022;129:109341.
125. Sha W, Guo F. Thermal transport in two-dimensional carbon nitrides: a comparative molecular dynamics study. *Carbon Trends*. 2022;7:100161.
126. Wang X, Wang Y, Wang J, et al. Pressure stabilized lithium-aluminum compounds with both superconducting and superionic behaviors. *Phys Rev Lett*. 2022;129(24):246403.
127. Wu X, Han Q. Transition from incoherent to coherent phonon thermal transport across graphene/h-BN van der Waals superlattices. *Int J Heat Mass Tran*. 2022;184:122390.
128. Wu X, Han Q. Maximum thermal conductivity of multilayer graphene with periodic two-dimensional empty space. *Int J Heat Mass Tran*. 2022;191:122829.
129. Wu X, Han Q. Tunable anisotropic in-plane thermal transport of multilayer graphene induced by 2D empty space: insights from interfaces. *Surf Interfaces*. 2022;33:102296.
130. Xu K, Liang T, Fu Y, et al. Gradient nano-grained graphene as 2D thermal rectifier: a molecular dynamics based machine learning study. *Appl Phys Lett*. 2022;121(13):133501.
131. Ying P, Liang T, Du Y, Zhang J, Zeng X, Zhong Z. Thermal transport in planar sp<sup>2</sup>-hybridized carbon allotropes: a comparative study of biphenylene network, pentaheptite and graphene. *Int J Heat Mass Tran*. 2022;183:122060.
132. Zhou Z, Xu K, Song Z, et al. Isotope doping-induced crossover shift in the thermal conductivity of thin silicon nanowires. *J Phys Condens Matter*. 2022;35(8):085702.
133. Bea E, Viotti AM, Carusela M, Monastra A, Soba A. Assessment, improvement, and comparison of different computational tools used for the simulation of heat transport in nanostructures. *Simulation*. 2023;99(3):237-244.
134. Cheng R, Shen X, Klotz S, et al. Lattice dynamics and thermal transport of PbTe under high pressure. *Phys Rev B*. 2023;108(10):104306.
135. Cheng Y, Fan Z, Zhang T, et al. Magic angle in thermal conductivity of twisted bilayer graphene. *Mater Today Phys*. 2023;35:101093.
136. de Vries IF, Osthues H, Doltsinis NL. Thermal conductivity across transition metal dichalcogenide bilayers. *iScience*. 2023;26(4):106447.
137. Dong H, Cao C, Ying P, Fan Z, Qian P, Su Y. Anisotropic and high thermal conductivity in monolayer quasi-hexagonal fullerene: a comparative study against bulk phase fullerene. *Int J Heat Mass Tran*. 2023;206:123943.
138. Du P-H, Zhang C, Li T, Sun Q. Low lattice thermal conductivity with two-channel thermal transport in the superatomic crystal PH<sub>4</sub>AlBr<sub>4</sub>. *Phys Rev B*. 2023;107(15):155204.
139. Eriksson F, Fransson E, Linderalv C, Fan Z, Erhart P. Tuning the through-plane lattice thermal conductivity in van der Waals structures through rotational (dis) ordering. *ACS Nano*. 2023;17(24):25565-25574.
140. Fransson E, Rahm JM, Wiktor J, Erhart P. Revealing the free energy landscape of halide perovskites: metastability and transition characters in CsPbBr<sub>3</sub> and MAPbI<sub>3</sub>. *Chem Mater*. 2023;35(19):8229-8238.
141. Fransson E, Rosander P, Eriksson F, Rahm JM, Tadano T, Erhart P. Limits of the phonon quasi-particle picture at the cubic-to-tetragonal phase transition in halide perovskites. *Commun Phys*. 2023;6(1):173.
142. Fransson E, Wiktor J, Erhart P. Phase transitions in inorganic halide perovskites from machine-learned potentials. *J Phys Chem C*. 2023;127(28):13773-13781.
143. Li Y, Jiang J-W. Vacancy defects impede the transition from peapods to diamond: a neuroevolution machine learning study. *Phys Chem Chem Phys*. 2023;25(37):25629-25638.
144. Liang T, Ying P, Xu K, et al. Mechanisms of temperature-dependent thermal transport in amorphous silica from machine-learning molecular dynamics. *Phys Rev B*. 2023;108(18):184203.
145. Liu Y, Liu Y, Yue J, Xiong L, Nian L-L, Hu S. Modulation of interface modes for resonance-induced enhancement of the interfacial thermal conductance in pillar-based Si/Ge nanowires. *Phys Rev B*. 2023;108(23):235426.
146. Lu C, hui Li Z, Li S, et al. Molecular dynamics study of thermal transport properties across covalently bonded graphite-nanodiamond interfaces. *Carbon*. 2023;213:118250.
147. Lu Y, Shi Y, Wang J, Dong H, Yu J. Reduction of thermal conductivity in carbon nanotubes by fullerene encapsulation from machine-learning molecular dynamics simulations. *J Appl Phys*. 2023;134(24):244901.
148. Ouyang N, Zeng Z, Wang C, Wang Q, Chen Y. Role of high-order lattice anharmonicity in the phonon thermal transport of silver halide Ag X (X = Cl, Br, I). *Phys Rev B*. 2023;108(17):174302.
149. Pan S, Huang T, Vazan A, et al. Magnesium oxide-water compounds at megabar pressure and implications on planetary interiors. *Nat Commun*. 2023;14(1):1165.
150. Rosander P, Fransson E, Milesi-Brault C, et al. Anharmonicity of the antiferrodistortive soft mode in barium zirconate BaZrO<sub>3</sub>. *Phys Rev B*. 2023;108(1):014309.
151. Sha W, Dai X, Chen S, Yin B, Guo F. Phonon thermal transport in two-dimensional PbTe monolayers via extensive molecular dynamics simulations with a neuroevolution potential. *Mater Today Phys*. 2023;34:101066.

152. Shi J, Liang Z, Wang J, et al. Double-shock compression pathways from diamond to BC8 carbon. *Phys Rev Lett.* 2023;131(14):146101.
153. Shi Y-B, Chen Y-Y, Wang H, et al. Investigation of the mechanical and transport properties of InGeX<sub>3</sub> (X = S, Se and Te) monolayers using density functional theory and machine learning. *Phys Chem Chem Phys.* 2023;25(20):13864-13876.
154. Shi Y, Chen Y, Dong H, Wang H, Qian P. Investigation of phase transition, mechanical behavior and lattice thermal conductivity of halogen perovskites using machine learning interatomic potentials. *Phys Chem Chem Phys.* 2023;25(44):30644-30655.
155. Su Y, Chen Y-Y, Wang H, et al. Origin of low lattice thermal conductivity and mobility of lead-free halide double perovskites. *J Alloys Compd.* 2023;962:170988.
156. Sun Z, Qi Z, Liang K, et al. A neuroevolution potential for predicting the thermal conductivity of  $\alpha$ ,  $\beta$ , and  $\epsilon$ -Ga<sub>2</sub>O<sub>3</sub>. *Appl Phys Lett.* 2023;123(19):192202.
157. Wang Y, Fan Z, Qian P, Caro MA, Ala-Nissila T. Quantum-corrected thickness-dependent thermal conductivity in amorphous silicon predicted by machine learning molecular dynamics simulations. *Phys Rev B.* 2023;107(5):054303.
158. Wang Q, Wang C, Chi C, et al. Phonon transport in freestanding SrTiO<sub>3</sub> down to the monolayer limit. *Phys Rev B.* 2023;108(11):115435.
159. Wei H, Hu Y, Bao H. Influence of point defects and multiscale pores on the different phonon transport regimes. *Commun Mater.* 2023;4:1.
160. Wiktor J, Fransson E, Kubicki D, Erhart P. Quantifying dynamic tilting in halide perovskites: chemical trends and local correlations. *Chem Mater.* 2023;35(17):6737-6744.
161. Wu X, Huang X, Yang L, et al. Suppressed thermal transport in mathematically inspired 2D heterosystems. *Carbon.* 2023;213:118264.
162. Wu X, Ying P, Li C, Han Q. Dual effects of hetero-interfaces on phonon thermal transport across graphene/C<sub>3</sub>N lateral superlattices. *Int J Heat Mass Tran.* 2023;201:123643.
163. Xiong J, Qi Z, Liang K, et al. Molecular dynamics insights on thermal conductivities of cubic diamond, lonsdaleite and nanotwinned diamond via the machine learned potential. *Chin Phys B.* 2023;32(12):128101.
164. Xu K, Hao Y, Liang T, et al. Accurate prediction of heat conductivity of water by a neuroevolution potential. *J Chem Phys.* 2023;158(20):204114.
165. Yang C, Wang J, Ma D, et al. Phonon transport across GaN-diamond interface: the nontrivial role of pre-interface vacancy-phonon scattering. *Int J Heat Mass Tran.* 2023;214:124433.
166. Ying P, Dong H, Liang T, Fan Z, Zhong Z, Zhang J. Atomistic insights into the mechanical anisotropy and fragility of monolayer fullerene networks using quantum mechanical calculations and machine-learning molecular dynamics simulations. *Extrem Mech Lett.* 2023;58:101929.
167. Ying P, Liang T, Xu K, et al. Variable thermal transport in black, blue, and violet phosphorene from extensive atomistic simulations with a neuroevolution potential. *Int J Heat Mass Tran.* 2023;202:123681.
168. Ying P, Liang T, Xu K, et al. Sub-micrometer phonon mean free paths in metal-organic frameworks revealed by machine-learning molecular dynamics simulations. *ACS Appl Mater Interfaces.* 2023;15(30):36412-36422.
169. Zhang H, Gu X, Fan Z, Bao H. Vibrational anharmonicity results in decreased thermal conductivity of amorphous HfO<sub>2</sub> at high temperature. *Phys Rev B.* 2023;108(4):045422.
170. Zhao R, Wang S, Kong Z, et al. Development of a neuroevolution machine learning potential of Pd-Cu-Ni-P alloys. *Mater Des.* 2023;231:112012.
171. Zhou Z, Zeng J, Song Z, et al. Thermal conductivity of fivefold twinned silicon-germanium heteronanowires. *Phys Chem Chem Phys.* 2023;25(37):25368-25376.
172. Berger E, Komsa H-P. Polarizability models for simulations of finite temperature Raman spectra from machine learning molecular dynamics. *Phys Rev Mater.* 2024;8(4):043802.
173. Berger E, Niemelä J, Lampela O, Juffer AH, Komsa H-P. Raman spectra of amino acids and peptides from machine learning polarizabilities. *J Chem Inf Model.* 2024;64(12):4601-4612.
174. Berrens ML, Kundu A, Calegari Andrade MF, Pham TA, Galli G, Donadio D. Nuclear quantum effects on the electronic structure of water and ice. *J Phys Chem Lett.* 2024;15(26):6818-6825.
175. Cao C, Cao S, Zhu Y, Dong H, Wang Y, Qian P. Thermal transports of 2D phosphorous carbides by machine learning molecular dynamics simulations. *Int J Heat Mass Tran.* 2024;224:125359.
176. Chen R, Tian Y, Cao J, Ren W, Hu S, Zeng C. Unified deep learning network for enhanced accuracy in predicting thermal conductivity of bilayer graphene, hexagonal boron nitride, and their heterostructures. *J Appl Phys.* 2024;135(14):145106.
177. Chen S, Jin X, Zhao W, Li T. Intricate short-range order in GeSn alloys revealed by atomistic simulations with highly accurate and efficient machine-learning potentials. *Phys Rev Mater.* 2024;8(4):043805.
178. Chen Z, Berrens ML, Chan K-T, Fan Z, Donadio D. Thermodynamics of water and ice from a fast and scalable first-principles neuroevolution potential. *J Chem Eng Data.* 2024;69(1):128-140.
179. Cheng R, Zeng Z, Wang C, Ouyang N, Chen Y. Impact of strain-insensitive low-frequency phonon modes on lattice thermal transport in A<sub>2</sub>XB<sub>6</sub>-type perovskites. *Phys Rev B.* 2024;109(5):054305.
180. Cheng Y, Zhang H, Xiong S, Volz S, Zhang T. Tuning the thermal resistance of SiGe phononic interfaces across ballistic and diffusive regimes. *Int J Heat Mass Tran.* 2024;235:126144.
181. Deng Q, Liu Q, Yuan M, et al. Acceleration of multi-body molecular dynamics with customized parallel dataflow. *IEEE Trans Parallel Distr Syst.* 2024;35(12):2297-2314.
182. Dong H, Shi Y, Ying P, et al. Molecular dynamics simulations of heat transport using machine-learned potentials: a mini-review and tutorial on GPUMD with neuroevolution potentials. *J Appl Phys.* 2024;135(16):161101.
183. Dong H, Li Z, Sun B, Zhou Y, Liu L, Yang J-Y. Thermal transport in disordered wurtzite ScAlN alloys using machine learning interatomic potentials. *Mater Today Commun.* 2024;39:109213.
184. Fan H, Ying P, Fan Z, Chen Y, Li Z, Zhou Y. Anomalous strain-dependent thermal conductivity in the metal-organic framework HKUST-1. *Phys Rev B.* 2024;109(4):045424.
185. Fang M, Tang S, Fan Z, Shi Y, Xu N, He Y. Transferability of machine learning models for predicting Raman spectra. *J Phys Chem A.* 2024;128(12):2286-2294.
186. Feng HF, Liu B, Bai JL, Zhang X, Song ZX, Guo Z-X. Nontrivial impact of interlayer coupling on thermal conductivity: opposing trends in in-plane and out-of-plane phonons. *Phys Rev B.* 2024;110(21):214304.
187. Fine L, Lavén R, Wei Z, et al. Configuration and dynamics of hydride ions in the nitride-hydride catalyst Ca<sub>3</sub>CrN<sub>3</sub>H. *Chem Mater.* 2024;37(1):489-496.
188. Folkner DA, Chen Z, Barbalinardo G, Knoop F, Donadio D. Elastic moduli and thermal conductivity of quantum materials at finite temperature. *J Appl Phys.* 2024;136(22):221101.
189. Fransson E, Wiktor J, Erhart P. Impact of organic spacers and dimensionality on templating of halide perovskites. *ACS Energy Lett.* 2024;9(8):3947-3954.
190. Fransson E, Rosander P, Erhart P, Wahnström G. Understanding correlations in BaZrO<sub>3</sub>: structure and dynamics on the nanoscale. *Chem Mater.* 2024;36(1):514-523.
191. Gabourie AJ, Polanco CA, McClellan CJ, et al. AI-accelerated atoms-to-circuits thermal simulation pipeline for integrated circuit design. In: *2024 IEEE International Electron Devices Meeting (IEDM)*; 2024:1-4.
192. Huang G, Zhang L, Chu S, Xie Y, Chen Y. A highly ductile carbon material made of triangle rings: a study of machine learning. *Appl Phys Lett.* 2024;124(4):043103.
193. Huang X, Li C, Yuan M, Shuai J, Li X-G, Hou Y. Unphysical grain size dependence of lattice thermal conductivity in Mg<sub>3</sub>(Sb, Bi)<sub>2</sub>: an atomistic view of concentration dependent segregation effects. *Mater Today Phys.* 2024;43:101386.

194. Li G, Tang J, Zheng J, et al. Convergent thermal conductivity in strained monolayer graphene. *Phys Rev B*. 2024;109(3):035420.
195. Li H, Zhu Y, Chu M, Dong H, Zhang G. Thermal conductivity of irregularly shaped nanoparticles from equilibrium molecular dynamics. *J Phys Condens Matter*. 2024;36(34):345703.
196. Li K, Liu B, Zhou J, Sun Z. Revealing the crystallization dynamics of Sb-Te phase change materials by large-scale simulations. *J Mater Chem C*. 2024;12(11):3897-3906.
197. Li Y, Guo Y, Xiong S, Yi H. Enhanced heat transport in amorphous silicon via microstructure modulation. *Int J Heat Mass Tran*. 2024;222:125167.
198. Li Z, Dong H, Wang J, Liu L, Yang J-Y. Active learning molecular dynamics-assisted insights into ultralow thermal conductivity of two-dimensional covalent organic frameworks. *Int J Heat Mass Tran*. 2024;225:125404.
199. Li Z, Wang J, Dong H, Zhou Y, Liu L, Yang J-Y. Mechanistic insights into water filling effects on thermal transport of carbon nanotubes from machine learning molecular dynamics. *Int J Heat Mass Tran*. 2024;235:126152.
200. Liu Y, Meng H, Zhu Z, Yu H, Zhuang L, Chu Y. Predicting mechanical and thermal properties of high-entropy ceramics via transferable machine-learning-potential-based molecular dynamics. *Adv Funct Mater*. 2024;35(16):2418802.
201. Lyu S, Cheng R, Li H, Chen Y. Effects of local chemical ordering on the thermal transport in entropy-regulated PbSe-based thermoelectric materials. *Appl Phys Lett*. 2024;124(23):232202.
202. Muhammed MM, Molkath JH. Thermal characteristics of CsPbX<sub>3</sub> (X = Cl/Br/I) halide perovskites. *Mater Today Commun*. 2024;41:110628.
203. de Araujo Oliveira H, Fan Z, Harju A, Pereira LFC. Tuning the thermal conductivity of silicon phononic crystals via defect motifs: implications for thermoelectric devices and photovoltaics. *ACS Appl Nano Mater*. 2025;8(9):4364-4372.
204. Pegolo P, Grasselli F. Thermal transport of glasses via machine learning driven simulations. *Frontiers in Materials*. 2024;11:1369034.
205. Qi Z, Sun X, Sun Z, et al. Interfacial optimization for AlN/diamond heterostructures via machine learning potential molecular dynamics investigation of the mechanical properties. *ACS Appl Mater Interfaces*. 2024;16(21):27998-28007.
206. Ru G, Qi W, Sun S, Tang K, Du C, Liu W. Interlayer friction and adhesion effects in penta-PdSe<sub>2</sub>-based van der Waals heterostructures. *Adv Sci*. 2024;11(34):2400395.
207. Schäfer C, Fojt J, Lindgren E, Erhart P. Machine learning for polaritonic chemistry: accessing chemical kinetics. *J Am Chem Soc*. 2024;146(8):5402-5413.
208. Shi P, Xu Z. Exploring fracture of H-BN and graphene by neural network force fields. *J Phys Condens Matter*. 2024;36(41):415401.
209. So S, Lee J-H. Unraveling interfacial thermal transport in  $\beta$ -Ga<sub>2</sub>O<sub>3</sub>/h-BN van der Waals heterostructures. *Mater Today Phys*. 2024;46:101506.
210. So S, Seol JH, Lee J-H. Quasiballistic thermal transport in submicron-scale graphene nanoribbons at room-temperature. *Nano-scale Adv*. 2024;6(11):2919-2927.
211. Sonti S, Sun C, Chen Z, et al. Stability and dynamics of zeolite-confined gold nanoclusters. *J Chem Theor Comput*. 2024;20(18):8261-8269.
212. Sun C, Goel R, Kulkarni AR. Developing cheap but useful machine learning-based models for investigating high-entropy alloy catalysts. *Langmuir*. 2024;40(7):3691-3701.
213. Sun Z, Sun X, Qi Z, et al. Investigating thermal transport across the AlN/diamond interface via the machine learning potential. *Diam Relat Mater*. 2024;147:111303.
214. Sun Z, Zhang D, Qi Z, et al. Insight into interfacial heat transfer of  $\beta$ -Ga<sub>2</sub>O<sub>3</sub>/diamond heterostructures via the machine learning potential. *ACS Appl Mater Interfaces*. 2024;16(24):31666-31676.
215. Tang J, Zheng J, Song X, Cheng L, Guo R. In-plane thermal conductivity of hexagonal boron nitride from 2D to 3D. *J Appl Phys*. 2024;135(20):205105.
216. Tang Z, Wang X, He C, et al. Effects of thermal expansion and four-phonon interactions on the lattice thermal conductivity of the negative thermal expansion material ScF<sub>3</sub>. *Phys Rev B*. 2024;110(13):134320.
217. Tian H, Dong W, Zhang W, Guo C. Machine learning techniques to probe the properties of molten salt phase change materials for thermal energy storage. *Cell Rep Phys Sci*. 2024;5(7):102042.
218. Tian W, Wang C, Zhou K. The dynamic diversity and invariance of ab initio water. *J Chem Theory Comput*. 2024;20(23):10667-10675.
219. Timalisina B, Nguyen HG, Esfarjani K. Neuroevolution machine learning potential to study high temperature deformation of entropy-stabilized oxide MgNiCoCuZnO<sub>5</sub>. *J Appl Phys*. 2024;136(15):155109.
220. Wan J, Li G, Guo Z, Qin H. Thermal transport in C<sub>6</sub>N<sub>7</sub> monolayer: a machine learning based molecular dynamics study. *J Phys Condens Matter*. 2024;37(2):025301.
221. Wang B, Ying P, Zhang J. The thermoelastic properties of monolayer covalent organic frameworks studied by machine-learning molecular dynamics. *Nanoscale*. 2024;16(1):237-248.
222. Wang C, Tian W, Zhou K. Ab initio simulation of liquid water without artificial high temperature. *J Chem Theor Comput*. 2024;20:8202.
223. Wang R, Yu H, Zhong Y, Xiang H. Identifying direct bandgap silicon structures with high-throughput search and machine learning methods. *J Phys Chem C*. 2024;128(30):12677-12685.
224. Wang X, Yang J, Ying P, Fan Z, Zhang J, Sun H. Dissimilar thermal transport properties in  $\kappa$ -Ga<sub>2</sub>O<sub>3</sub> and  $\beta$ -Ga<sub>2</sub>O<sub>3</sub> revealed by homogeneous nonequilibrium molecular dynamics simulations using machine-learned potentials. *J Appl Phys*. 2024;135(6):065104.
225. Wei P, Liu Y, Liu Y, Zhuang L, Yu H, Chu Y. High-throughput composition screening of high-entropy rare-earth monosilicates for superior CMAS corrosion resistance up to 1873 K. *Corros Sci*. 2024;235:112172.
226. Wu S, Kang D, Yu X, Dai J. Thermal transport across armchair-zigzag graphene homointerface. *Appl Phys Lett*. 2024;125(14):142206.
227. Wu X, Cheng Y, Huang S, Xiong S. Phonon resonance effect and defect scattering in covalently bonded carbon nanotube networks. *Phys Rev Appl*. 2024;22(2):024038.
228. Wu X, Zhou W, Dong H, et al. Correcting force error-induced underestimation of lattice thermal conductivity in machine learning molecular dynamics. *J Chem Phys*. 2024;161(1):014103.
229. Wu X, Wu Y, Huang X, et al. Isotope interface engineering for thermal transport suppression in cryogenic graphene. *Mater Today Phys*. 2024;46:101500.
230. Wu Z, Liu R, Wei N, Wang L. Unexpected reduction in thermal conductivity observed in graphene/h-BN heterostructures. *Phys Chem Chem Phys*. 2024;26(5):3823-3831.
231. Xu F, Wang D, Li Z, et al. Large-scale simulation of thermal conductivity in CaSiO<sub>3</sub> perovskite with neuroevolution potential. *Appl Phys Lett*. 2024;125(3):034104.
232. Xu N, Rosander P, Schäfer C, et al. Tensorial properties via the neuroevolution potential framework: fast simulation of infrared and Raman spectra. *J Chem Theor Comput*. 2024;20(8):3273-3284.
233. Yan Z, Zhu Y. Impact of lithium nonstoichiometry on ionic diffusion in tetragonal garnet-type Li<sub>7</sub>La<sub>3</sub>Zr<sub>2</sub>O<sub>12</sub>. *Chem Mater*. 2024;36(23):11551-11557.
234. Yang N, Chen R, Liu Y, Ren W, Hu S. Numerical evaluation of the effect of the twist angle on phonon hydrodynamics in twisted bilayer graphene. *Phys Rev B*. 2024;110(24):245305.
235. Ying P, Natan A, Hod O, Urbakh M. Effect of interlayer bonding on superlubric sliding of graphene contacts: a machine-learning potential study. *ACS Nano*. 2024;18(14):10133-10141.
236. Yu L, Dong K, Yang Q, et al. Dynamic mesophase transition induces anomalous suppressed and anisotropic phonon thermal transport. *NPJ Comput Mater*. 2024;10:1.
237. Yu M, Zhao Z, Guo W, Zhang Z. Fracture toughness of two-dimensional materials dominated by edge energy anisotropy. *J Mech Phys Solid*. 2024;186:105579.

238. Yue J, Hu S, Xu B, et al. Unraveling the mechanisms of thermal boundary conductance at the graphene-silicon interface: insights from ballistic, diffusive, and localized phonon transport regimes. *Phys Rev B*. 2024;109(11):115302.
239. Zeraati M, Oganov AR, Fan T, Solodovnikov SF. Searching for low thermal conductivity materials for thermal barrier coatings: a theoretical approach. *Phys Rev Mater*. 2024;8(3):033601.
240. Zhang C, Sun J, Cheng J, Wang Q. Ultralow lattice thermal conductivity in quasi-one-dimensional BiI<sub>3</sub> with suppressed phonon coherence. *Phys Rev B*. 2024;110(17):174309.
241. Zhang G, Zhao S, Qin H, Liu Y. A unified strength criterion of diamane grain boundaries. *Extrem Mech Lett*. 2024;68:102146.
242. Zhang J, Zhang H-C, Li W, Zhang G. Thermal conductivity of GeTe crystals based on machine learning potentials. *Chin Phys B*. 2024;33(4):047402.
243. Zhang J, Zhang O, Bonati L, Hou T. Combining transition path sampling with data-driven collective variables through a reactivity-biased shooting algorithm. *J Chem Theor Comput*. 2024;20(11):4523-4532.
244. Zhang Z, Lu Q, Ding C, et al. Crystal structure prediction of lithium-beryllium alloys under pressure with distinctive electronic and dynamic behaviors. *Phys Rev B*. 2024;110(17):174101.
245. Zhao Z, Yi M, Guo W, Zhang Z. General-purpose neural network potential for Ti-Al-Nb alloys towards large-scale molecular dynamics with ab initio accuracy. *Phys Rev B*. 2024;110(18):184115.
246. Zhou W, Song B. Isotope effect on four-phonon interaction and lattice thermal transport: an atomistic study of lithium hydride. *Phys Rev B*. 2024;110(20):205202.
247. Quek A, Ouyang N, Lin H-M, Delaire O, Guilleminot J. Enhancing robustness in machine-learning-accelerated molecular dynamics: a multi-model nonparametric probabilistic approach. *Mech Mater*. 2025;202:105237.
248. Bao Y, Chen T, Miao Z, et al. Machine-learning-assisted understanding of depth-dependent thermal conductivity in lithium niobate induced by point defects. *Adv Electron Mater*. 2025:2400944.
249. Bro-Jørgensen W, Hamill JM, Donadio D, Solomon GC. Bridging the Gap: Using Machine Learning Force Fields to Simulate Gold Break Junctions at Pulling Speeds Closer to Experiments. *ChemRxiv*. 2025.
250. Cao C, Bai L, Cao S, et al. Structural and transport properties of LiTFSI/G3 electrolyte with machine-learned molecular dynamics. *J Phys Chem C*. 2025;129(28):13030-13039.
251. Cao S, Wang A, Fan Z, et al. Lattice thermal conductivity of 16 elemental metals from molecular dynamics simulations with a unified neuroevolution potential. *J Appl Phys*. 2025;137(22):225101.
252. Chen Z, Yuan Y, Wang Y, et al. Softening of vibrational modes and anharmonicity induced thermal conductivity reduction in a-Si:H at high temperatures. *Adv Electron Mater*. 2025:2500104.
253. Chen F, Wang H, Jiang Y, Zhan L, Yang Y. Development of a neuroevolution machine learning potential of Al-Cu-Li alloys. *Metals*. 2025;15(1):48.
254. Chen Z, Yuan Y, Ding W, Li S, An M, Zhang G. Hyperparameter optimization and force error correction of neuroevolution potential for predicting thermal conductivity of wurtzite GaN. *Chin Phys B*. 2025.
255. Cheng R, Wang C, Ouyang N, Shen X, Chen Y. Strong crystalline thermal insulation induced by extended antibonding states. *arXiv:2505.06926 [cond-mat.mtrl-sci]*. 2025.
256. Dai J-P, Liu X, Li D. Insight into structural-functional relationship for conductive-radiative heat transfer in multi-scale thermal insulating carbon aerogels. *Carbon*. 2025;243:120467.
257. Donadio D, Berrens ML, Zhao W, Chen S, Li T. Metastability and Ostwald step rule in the crystallisation of diamond and graphite from molten carbon. *Nat Commun*. 2025;16(1):6324.
258. Du P-H, Wang Q, Sun Q, Jena P. Thermal rectification of sierpiński tetrahedron fractals assembled from supertetrahedral T<sub>2</sub>-type tin selenide clusters. *Phys Rev B*. 2025;111(12):L121406.
259. Feng X, Pan S, Katagiri K, et al. Nanosecond structural evolution in shocked coesite. *Sci Adv*. 2025;11(17):eads3139.
260. Hainer T, Fransson E, Dutta S, Wiktor J, Erhart P. A morphotropic phase boundary in MA<sub>1-x</sub>FA<sub>x</sub>PbI<sub>3</sub>: linking structure, dynamics, and electronic properties. *arXiv:2503.22372 [cond-mat.mtrl-sci]*. 2025.
261. Hao Y, Che J, Wang X, et al. Copper delocalization leads to ultralow thermal conductivity in chalcogenide CuBiSeCl<sub>2</sub>. *Phys Rev B*. 2025;111(19):195207.
262. Hu Z-Q, Xie Y-F, Liu R, Shao J-L, Chen P-W. Prediction of reaction kinetics for CL-20 and host-guest crystals under high temperature and pressure using neuroevolution potential. *J Chem Phys*. 2025;162(17):174503.
263. Hu S, Gu X. Approaching to low thermal conductivity limit in layered materials through full-spectrum phonon band engineering. *Mater Today Phys*. 2025;52:101669.
264. Jia X, Bao Y, Cao S, Su Y, Qian P. Temperature effects on radiation damage in hcp-zirconium: a molecular dynamics study using a fine-tuned machine-learned potential. *SSRN*. 2025:156025.
265. Jiang W, Liang T, Xu J, Ouyang W. Strain-engineered anisotropic thermal transport in layered MoS<sub>2</sub> structures. *ACS Appl Mater Interfaces*. 2025;17(23):34833-34844.
266. Jiang W, Bu H, Liang T, et al. Accurate modeling of interfacial thermal transport in van der Waals heterostructures via hybrid machine learning and registry-dependent potentials. *arXiv:2505.00376 [physics]*. 2025.
267. Kayastha P, Fransson E, Erhart P, Whalley L. Octahedral tilt-driven phase transitions in BaZrS<sub>3</sub> chalcogenide perovskite. *J Phys Chem Lett*. 2025;16(8):2064-2071.
268. Lavén R, Fransson E, Erhart P, Juranyi F, Granroth GE, Karlsson M. Unraveling the nature of vibrational dynamics in CsPbI<sub>3</sub> by inelastic neutron scattering and molecular dynamics simulations. *J Phys Chem Lett*. 2025;16(19):4812-4818.
269. Li K, Ma H. Decoding the thermal conductivity of ionic covalent organic frameworks: optical phonons as key determinants revealed by neuroevolution potential. *Mater Today Phys*. 2025;54:101724.
270. Li Z, Han L, Ouyang T, Cao J, Yao Y, Wei X. Thermal and mechanical properties of deep-ultraviolet light sources candidate materials BeGeN<sub>2</sub> by machine-learning molecular dynamics simulations. *Phys Rev Mater*. 2025;9(3):033804.
271. Li S, Fang L, Liu T, et al. Machine learning-accelerated molecular dynamics calculations for investigating the thermal modulation by ferroelectric domain wall in KTN single crystals. *Comput Mater Sci*. 2025;249:113674.
272. Li X, Liu R, Hou J, Zhang Z, Zhang Z. Trade-off model for strength-ductility relationship of metallic materials. *Acta Mater*. 2025;289:120942.
273. Liang T, Xu K, Ying P, et al. Probing the ideal limit of interfacial thermal conductance in two-dimensional van der Waals heterostructures. *arXiv:2502.13601 [physics.comp-ph]*. 2025.
274. Linderålv C, Österbacka N, Wiktor J, Erhart P. Optical line shapes of color centers in solids from classical autocorrelation functions. *npj Comput Mater*. 2025;11(1):101.
275. Lindgren E, Jackson AJ, Fransson E, et al. Predicting neutron experiments from first principles: a workflow powered by machine learning. *J Mater Chem A*. 2025.
276. Liu Y-Q, Dong H-K, Ren Y, Zhang W-G, Chen W. Crystallization of h-BN by molecular dynamics simulation using a machine learning interatomic potential. *Comput Mater Sci*. 2025;249:113621.
277. Liu J, Zhang L. A physics-informed machine learning perspective to present the structures and properties of titanium matrixes and nanoclusters through atomic modeling. *Nanoscale*. 2025;17(18):11482-11501.
278. Liu Z, Sha J, Song G-L, Wang Z, Zhang Y. Understanding magnesium dissolution through machine learning molecular dynamics. *Chem Eng J*. 2025;516:163578.
279. Liu J, Yin Q, He M, Zhou J. Constructing accurate machine learned potential and performing highly efficient atomistic simulation to

- predict structural and thermal properties: the case of  $\text{Cu}_7\text{PS}_6$ . *Comput Mater Sci.* 2025;251:113686.
280. Liu Y, Fu Y, Gu F, Yu H, Zhuang L, Chu Y. Lattice-distortion-driven reduced lattice thermal conductivity in high-entropy ceramics. *Adv Sci.* 2025;12(19):2501157.
281. Liu F, Mao R, Liu Z, Du J, Gao P. Probing phonon transport dynamics across an interface by electron microscopy. *Nature.* 2025;642(8069):941-946.
282. Lu C, Li Z, Sang X, et al. Stress-driven grain boundary structural transition in diamond by machine learning potential. *Small.* 2025;21(16):2409092.
283. Lu C, Xu X, Cheng Y, et al. Interfacial thermal conductance at the gas-solid interface: microscopic energy transport mechanisms and the thermal rectification phenomenon. *Int Commun Heat Mass Tran.* 2025;166:109153.
284. Luo W, Yin E, Wang L, Lian W, Wang N, Li Q. Heat transfer enhancement of N-Ga-Al semiconductors heterogeneous interfaces. *Int J Heat Mass Tran.* 2025;244:126902.
285. Lyu S, Cao X, Zhou Y, Chen Y. Phonon scattering and thermal transport in PbSe and medium entropy thermoelectric  $\text{PbSe}_{0.5}\text{Te}_{0.25}\text{S}_{0.25}$  with defects of different dimensions. *J Phys Chem Lett.* 2025;5429.
286. Moon J, Tian Z. Crystal-like thermal transport in amorphous carbon. *npj Comput Mater.* 2025;11:1.
287. Oh M-H, Kim H-S, Cho S. Effects of wide phononic bandgaps on thermal conductance in silicon nanomeshes. *J Phys Chem C.* 2025;129(8):4183-4191.
288. Ouyang N, Shen D, Wang C, Cheng R, Wang Q, Chen Y. Positive temperature-dependent thermal conductivity induced by wavelike phonons in complex Ag-based argyrodites. *Phys Rev B.* 2025;111(6):064307.
289. Pegolo P, Drigo E, Grasselli F, Baroni S. Transport coefficients from equilibrium molecular dynamics. *J Chem Phys.* 2025;162(6):064111.
290. Rosander P, Fransson E, Österbacka N, Erhart P, Wahnström G. Untangling the Raman spectra of cubic and tetragonal  $\text{BaZrO}_3$ . *Phys Rev B.* 2025;111:064107.
291. Seifi A, Ghasemi M, Kateb M, Marashi P. Challenges in determining the thermal conductivity of core-shell nanowires by atomistic simulation. *J Chem Phys.* 2025;162(12):124706.
292. Sun Z, Song Y, Qi Z, et al. Heat transport exploration through the GaN/diamond interfaces using machine learning potential. *Int J Heat Mass Tran.* 2025;241:126724.
293. Sun X, Lu S, Shan S, Zhang Z, Chen J. Origin of superdiffusive thermal transport in one-dimensional van der Waals atomic chains. *Phys Rev B.* 2025;111(20):205404.
294. Sun J, Li X, Li T, et al. Sliding and superlubric moiré twisting ferroelectric transition in  $\text{HfO}_2$ . *arXiv:2505.08164 [cond-mat.mtrl-sci]*. 2025.
295. Tan Z, Wang S, Liu Y, et al. Coherent and incoherent phonon transport in graphene/h-BN superlattice: a machine learning potential. *Phys E Low-dimens Syst Nanostruct.* 2025;172:116259.
296. Tuchinda N, Schuh CA. Grain boundary segregation spectra from a generalized machine-learning potential. *Scr Mater.* 2025;264:116682.
297. Wang Y, Fan Z, Qian P, Caro MA, Ala-Nissila T. Density dependence of thermal conductivity in nanoporous and amorphous carbon with machine-learned molecular dynamics. *Phys Rev B.* 2025;111(9):094205.
298. Wang L-D, Cheng Y-B, Zhou J. Molecular dynamics study on phonon coherent transport in III-V semiconductor superlattices. *J Appl Phys.* 2025;137(11):115103.
299. Wang Y, Wang J, Yao G, et al. Phase transitions and dimensional cross-over in layered confined solids. *Proc Natl Acad Sci.* 2025;122(17):e2502980122.
300. Wang X, Wu X, Ying P, Fan Z, Sun H. Interface phonon modes governing the ideal limit of thermal transport across diamond/cubic boron nitride interfaces. *arXiv:2504.18473 [cond-mat.mtrl-sci]*. 2025.
301. Wang Y, Xie L, Yang H, et al. Strong orbital-lattice coupling induces glassy thermal conductivity in high-symmetry single crystal  $\text{BaTiS}_3$ . *Phys Rev X.* 2025;15(1):011066.
302. Wang B, Li K, Zhang W, Sun Y, Zhou J, Sun Z. Thermal transport of  $\text{GeTe/Sb}_2\text{Te}_3$  superlattice by large-scale molecular dynamics with machine-learned potential. *J Phys Chem C.* 2025;129(13):6386-6396.
303. Wang B, Wang B, Yan H, Cai Y. Oxygen vacancy-driven interfacial alloying and mixing for enhanced heat transfer in gallium oxide. *Mater Today Phys.* 2025;54:101714.
304. Wen Z, Liu Y, Yang J, et al. Exceptional oxidation resistance of high-entropy carbides up to 3600°C. *Adv Mater.* 2025:2507254.
305. Wu X, Wu Z, Liang T, et al. Phonon coherence and minimum thermal conductivity in disordered superlattices. *Phys Rev B.* 2025;111(8):085413.
306. Xiao Y, Liu Y, Zhang ZTB, et al. Optimizing thermoelectric performance of graphene antidot lattices via quantum transport and machine-learning molecular dynamics simulations. *arXiv:2504.17450 [cond-mat.mes-hall]*. 2025.
307. Xiao F, Xie Q-Y, Yu R, Li H, Zhang J, Wang B-T. Impact of lattice distortions and overdamped vibrations on the structural properties and thermal transport of strongly anharmonic  $\text{AgSnSbTe}_3$  crystals. *Phys Rev B.* 2025;111(18):184304.
308. Xu B, Bai L, Xu S, Wu Q. Observing nucleation and crystallization of rocksalt LiF from molten state through molecular dynamics simulations with refined machine-learned force field. *J Chem Phys.* 2025;162(23):234705.
309. Xu X, Wang S, Qin H, et al. A high-efficiency neuroevolution potential for tobermorite and calcium silicate hydrate systems with ab initio accuracy. *arXiv:2505.18993 [cond-mat.mes-hall]*. 2025.
310. Yan Z, Fan Z, Zhu Y. Improving robustness and training efficiency of machine-learned potentials by incorporating short-range empirical potentials. *arXiv:2504.15925 [cond-mat.mtrl-sci]*. 2025.
311. Yang J, Zhu X, McGaughey AJH, Ang YS, Ong W-L. Two-mode terms in Wigner transport equation elucidate anomalous thermal transport in amorphous silicon. *Phys Rev B.* 2025;111(9):094206.
312. Yuan W-Z, Guo Y, Yi H-L. Consistency between the Green-Kubo formula and Lorentz model for predicting the infrared dielectric function of polar materials. *Phys Rev B.* 2025;111(18):184310.
313. Yue J, Chen R, Ma D, Hu S. Nanoparticle-assisted phonon transport modulation in Si/Ge heterostructures using neuroevolution potential machine learning models. *Chin Phys Lett.* 2025;42(3):036301.
314. Zeng Z, Fan Z, Simoncelli M, et al. Lattice distortion leads to glassy thermal transport in crystalline  $\text{Cs}_3\text{Bi}_2\text{I}_6\text{Cl}_3$ . *arXiv:2407.18510 [cond-mat.mtrl-sci]*. 2024.
315. Zeraati M, Oganov AR, Maltsev AP, Solodovnikov SF. Computational screening of complex oxides for next-generation thermal barrier coatings. *J Appl Phys.* 2025;137(6):065106.
316. Zhang X, Xie Y, Tao F, Sun C, Tang D. Thermal transport in  $\text{MoSi}_2\text{N}_4$  monolayer: a molecular dynamics study based on machine learning. *Int J Heat Mass Tran.* 2025;250:127290.
317. Zhang H, Cheng M, Jiang X, et al. Neuroevolution potential for thermal transport in silicon carbide. *J Mater Informatics.* 2025;5(3):34.
318. Zhang S, Chen P, Wei L, et al. Theoretical investigation on the dynamic thermal transport properties of graphene foam by machine-learning molecular dynamics simulations. *Int J Therm Sci.* 2025;210:109631.
319. Zhang C, Chen Y, Wang Q, Jena P. Phonon localization and a boson-peak-like anomaly in twisted penta-PdSe<sub>2</sub> bilayer. *Nano Lett.* 2025;25(21):8689-8695.
320. Zhang P, Zhang S, Qin Y, Du T, Wei L, Li X. Thermal switching characteristics and mechanism in multi-scale graphene foam composites: a machine-learning-based molecular dynamics exploration. *SSRN.* 2025.
321. Zhang L, Luo W, Liu R, Chen M, Yan Z, Cao K. Exploring the energy landscape of aluminas through machine learning interatomic potential. *Phys Rev Mater.* 2025;9(2):023801.

322. Zhang Y, Li M, Xie F, et al. Synergetic strength-ductility enhancement of bcc W wires by coherent oxide nanocomposites pinning effect. *Compos B Eng.* 2025;302:112558.
323. Zhang Z, Luo J, Wu H, Ma H, Zhu Y. Unveiling the microscopic origin of anomalous thermal conductivity in amorphous carbon. *Sci Adv.* 2025;11(23):eadx5007.
324. Zhou X, Liu Y, Tang B, et al. Million-atom heat transport simulations of polycrystalline graphene approaching first-principles accuracy enabled by neuroevolution potential on desktop GPUs. *J Appl Phys.* 2025;137(1):014305.
325. Zhou X, Xu Y, Chen Y, Tian F. Mechanism on lattice thermal conductivity of carbon-vacancy and porous medium entropy ceramics. *Scr Mater.* 2025;259:116568.
326. Zhou W, Liang N, Wu X, Xiong S, Fan Z, Song B. Insight into the effect of force error on the thermal conductivity from machine-learned potentials. *Mater Today Phys.* 2025;50:101638.
327. Zhou W, Liang N, Xiao W, Tong Z, Tian F, Song B. Ultrahigh interfacial thermal conductance for cooling gallium oxide electronics using cubic boron arsenide. *arXiv:2501.11082 [cond-mat.mtrl-sci]*. 2025.
328. Zhou W, Liu S. Two-dimensional ferroelectric crystal with temperature-invariant ultralow thermal conductivity. *arXiv:2501.09990 [cond-mat.mtrl-sci]*. 2025.
329. Zhu Z, Liu Y, Qin Y, et al. Tough and strong bioinspired high-entropy all-ceramics with a contiguous network structure. *Nat Commun.* 2025;16:1.
330. Fan Z, Garcia JH, Cummings AW, et al. Linear scaling quantum transport methodologies. *Phys Rep.* 2021;903:1-69.
331. Song Z, Han J, Henkelman G, Li L. Charge-optimized electrostatic interaction atom-centered neural network algorithm. *J Chem Theor Comput.* 2024;20(5):2088-2097.

## AUTHOR BIOGRAPHY

**Dr. Zheyong Fan** was born in 1983. He obtained a PhD in theoretical physics from Nanjing University in 2010. He was a postdoctoral researcher at Xiamen University and Aalto University. He is now a professor at Bohai University. He published a book on CUDA programming and a book on molecular dynamics. He developed the graphics processing units molecular dynamics (GPUMD) code for efficient molecular dynamics simulations with the neuroevolution potential (NEP) and the graphics processing units quantum transport (GPUQT) code for efficient linear-scaling quantum transport simulations.

**How to cite this article:** Xu K, Bu H, Pan S, et al. GPUMD 4.0: a high-performance molecular dynamics package for versatile materials simulations with machine-learned potentials. *Materials Genome Engineering Advances.* 2025;3(3):e70028. <https://doi.org/10.1002/mgea.70028>